Incorporating nuclear reactions into SEU prediction

Alex Hedlund

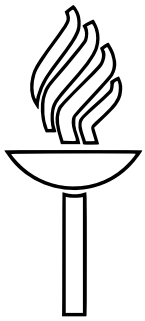

University of Jyväskylä
Department of Physics

Master's thesis

Approved by:
Arto Javanainen
Ari Virtanen

December 2011

Abstract

Space radiation can cause temporary and permanent damage to electronic components residing in outer space. The awareness of radiation environments in space and the knowledge of radiation effects is important for reliable design of space electronics used in, for example, satellites and spacecrafts.

Radiation-induced errors in the stored information of memory elements are called single-event upsets (SEU) and the prediction of SEUs is an important aspect of reliable space system design. The early, but still widely used, SEU rate prediction methods originating from the 1970s rely on the direct ionization, also called linear energy transfer (LET), of charged particles neglecting any other processes, such as nuclear reactions. Relying only on the LET means that similar particles always cause similar effect in the device. In reality, this is not true and the energy loss may vary significantly, especially in the case of a nuclear reaction, and this may lead to underestimation of the SEU rate and consequently cause the system to malfunction.

SEU rate prediction can also be made by utilizing physics-based particle transport simulators, such as the Geant4, where all physical processes can be included. For example, the significance of nuclear reactions in SEUs can be analyzed with the help of Geant4. However, the accuracy of such tools must be known in order to make reliable SEU rate predictions. In order to test the accuracy of the nuclear reaction description in Geant4, a time-of-flight (TOF) experiment was conducted in the RADEF facility. In these experiments, heavy ion beam was accelerated and guided onto heavy ion targets and the TOF and kinetic energy of the outcoming particles were measured. The same scenario was simulated by using Geant4 and the results for heavy fragment production were compared to those obtained from the experiments. The simulations show clear underestimation, by 1–2 orders of magnitude, in the heavy fragment production cross-sections. In order to improve the underlying code responsible for the nuclear physics, research on the low energy heavy ion reactions is required.

Despite the discrepancy between the Geant4 simulations and the experiments, the utilization of a particle transport simulator can improve the reliability of SEU rate prediction. In addition to LET, including other physical processes in SEU rate prediction makes it possible to assess situations which could not be analyzed with the traditional, LET-based, methods. One example of such a situation is a case where a signicifant amount of SEUs which are due to heavy fragments after nuclear reactions in the component.

Tiivistelmä

Avaruudessa on paljon sekä tunnettuja että tuntemattomia säteilylähteitä, ja säteily voi aiheuttaa sekä ohimeneviä että pysyviä häiriöitä avaruudessa oleville elektronisille komponenteille. Avaruuden erilaisten säteily-ympäristöjen sekä säteilyn vaikutusten tunteminen on siten tärkeää luotettavien, avaruuskäyttöön tarkoitettujen laitteiden, satelliittien tai avaruusalusten suunnittelussa.

Säteilyn aiheuttamaa muutosta muistielementin säilyttämässä informaatiossa kutsutaan single-event upsetiksi (SEU), ja niiden ennustaminen on yksi osa komponenttien säteilynkestävyyden arviointia. Ensimmäiset, mutta edelleen paljon käytetyt, 1970-luvulta peräisin olevat SEU-ennustukseen käytetyt menetelmät pohjautuvat varattujen hiukkasten suoraan ionisaatioon, nk. linear energy transferiin (LET), jättäen huomiotta muut prosessit, kuten ydinreaktiot. Näissä malleissa samanlaiset hiukkaset tai ytimet luovuttavat aina saman verran energiaa kulkiessaan saman matkan väliaineessa. Tämä ei kuitenkaan pidä todellisuudessa paikkaansa, sillä esimerkiksi ydinreaktion myötä hiukkanen voi luovuttaa komponentin säteilylle herkkään osaan huomattavasti suurempia energioita. Tämä tarkoittaa, että LET:n perusteella tietyssä säteily-ympäristössä kestäväksi todettu komponentti voikin toimia odottamattomasti.

SEU-ennustamista voidaan myös tehdä hyödyntämällä fysiikkapohjaisia, hiukkasen liikettä väliaineessa simuloivia ohjelmia, kuten Geant4:ää, jossa kaikki fysiikaaliset prosessit voidaan ottaa mukaan. Geant4:n avulla voidaan arvioida esim. ydinreaktioiden merkitystä komponentin SEU-herkkyteen. Simulaattoreiden tuottamien tulosten realistisuus on tunnettava hyvien SEU-ennusteiden saamiseksi. Tästä syystä suoritettiin RADEF-säteilytysasemalla lentoaikamittaus, jonka tuloksia voitaisiin vertailla Geant4:n antamiin tuloksiin.

Säteilytysaseman kokeissa ionisuihkuja, mm. ^{15}N ja ^{56}Fe, kiihdytettiin ja törmäytettiin kulta- ja wolframkohtioihin ja ulostulleiden hiukkasten lentoajat ja liike-energiat mitattiin. Vastaava tilanne simuloitiin Geant4:n avulla, ja suihkuhiukkasta raskaampien hiukkasten tuottoa vertailtiin kokeellisiin tuloksiin. Vertailu osoitti simulaation tuottavan raskaita fragmentteja selvästi, 1–2 kertaluokkaa, vähemmän kokeisiin nähden. Päätelmä siis on, että Geant4 sisältämien ydinreaktiomallien kehittäminen vaatii lisää tutkimusta ydinfysiikan ja eritoten matalaenergisten raskasionitörmäyksien osalta.

Huolimatta Geant4:sta ja kokeista saatujen tuloksien välisistä eroista, simulaattorin käyttäminen voi parantaa SEU-ennustamisen luotettavuutta. LET:n lisäksi muiden fysikaalisten prosessien huomioiminen SEU-ennustamisessa mahdollistaa sellaisten tapauksien arvioinnin, joissa SEUt tapahtuvat muun, kuin LET:n (suoran ionisaation) seurauksena ja joissa perinteiset menetelmät eivät siten toimisi. Tällaisia ovat mm. tilanteet, joissa SEUt aiheutuvat merkittäviltä osin komponentissa tapahtuvien ydinreaktioiden myötä syntyneistä, raskaista reaktiotuotteista.

Acknowledgements

I wish to express my appreciation and gratitude to my supervisors Arto Javanainen and Ari Virtanen without whom this thesis could not have been written. With strong dedication they have mentored me throughout the process of writing this thesis. I also want to thank professors Robert A. Weller and Robert A. Reed from the Vanderbilt University for the interesting technical discussions concerning Geant4.

Finally, I want to thank the guys in Holvi for the stimulating writing environment, and my family for their endless patience and support.

Contents

1 Introduction

In 1962, Wallmark and Marcus foresaw the semiconductor device failures from cosmic ray bombardment and predicted absolute limits to device size and packing density in order to prevent these problems [1]. Later that year, several satellites went out of service as a result of radiation generated by the US Air Force high-a6ltitude nuclear bomb experiments [2]. The first reports of unexpected behavior in communication satellite operation due to extra-terrestrial cosmic rays were published in 1975 [3]. Since then, the basic mechanisms of the variety of radiation effects in electronic components and the countermeasures against them have been under research. In this work, the main focus is on the single-event effects (SEE), the effects induced by the energy deposition of a single energetic particle.

The limits to device size and packing density proposed by Wallmark and Marcus have been exceeded long ago. A trend known as the Moore's law [4], which states that the amount of transistors in an integrated circuit doubles every two years, has been continuing until nowadays [5]. Many radiation hardening methods have been invented and successfully implemented but the continuous scaling of components increases the sensitivity to radiation introducing new challenges to radiation hardening techniques.

Usually, SEEs have been considered a problem only to spacecraft electronics. As modern aircrafts are increasingly reliant on microprocessors and memory devices, the knowledge of the natural radiation environments and the consequent effects in electronics has a big role also in the design of avionics systems. The risks of SEEs at sea level have received little attention, although Ziegler noted the potential susceptibility [6] soon after the discovery of the first SEEs in space. Studies by Normand show that secondary radiation, mainly neutrons, induced by cosmic rays cause SEEs also at ground level [7]. Similar results were also achieved earlier in private studies by memory chip vendors with the purpose of increasing the reliability of their products [8]. This implies that SEEs are of interest not solely in space applications, but also for manufacturers developing and producing terrestrial electronics.

In order to understand the occurrence of SEEs and to be able to design radiation hard components and systems, one must have adequate knowledge of the radiation environments to be able to predict where and when something could happen. In addition, the interactions of radiation with matter must be understood in order to predict what could happen. Accurate SEE prediction demands evaluation of all physical processes taking place in complex electronic devices residing in dynamic radiation environments. Analyzing the whole scenario analytically from the very bottom level to the top without major simplifications is an impractical task. However, results can be obtained with the aid of advanced computer models describing the effects at the low level (radiation in matter) as well as at the higher levels (circuit design, system geometries, radiation environments).

The traditional SEE rate prediction methods, which only include the energy deposition resulting from the direct ionization of incoming particles, have in many cases proven to be successful for older and bigger technologies. Despite the earlier success, relying on the average behavior of radiation when predicting the energy deposition in a device may not be adequate with future technologies. This work focuses on explaining the basics behind one type of SEE, the single-event upset (SEU) and the methods for predicting the SEU rate in a radiation environment. The traditional SEU rate prediction models as well as more advanced, physics simulator based SEU rate prediction methods are explained. In addition, a comparison between a particle transport simulator and an experiment is presented.

2 Physics and concepts related to the subject

2.1 Radiation and its interactions with matter

Radiation is energy which propagates through space or matter and it can be classified into *ionizing* and *non-ionizing* radiation depending on its ability to ionize the target atoms. Radiation can also be classified into *particle radiation* and *electromagnetic radiation*. Particle radiation consists of energetic subatomic particles whereas electromagnetic radiation consists of massless quanta of energy, called photons, propagating through space exhibiting wave-like behavior [9]. Radiation deposits energy in materials via electromagnetic and nuclear interactions which are explained in the following sections.

2.1.1 Electromagnetic interactions

The process where an atomic electron receives enough energy to be promoted to a higher energy level is called excitation. Ionization occurs if the energy transferred to the electron exceeds its binding energy, consequently ejecting the electron from the atom [9].

Both electromagnetic and particle radiation can be ionizing. Charged particles, such as beta, alpha or heavier particles, cause ionization mainly by interacting through Coulomb scattering with the atomic electrons of the medium. In the scattering process, the incident particle loses some fraction of its energy to atomic electrons, which are excited or entirely removed from the atom, leaving the target nucleus unchanged. This mechanism is known as the electronic stopping [10].

Electromagnetic radiation with frequency below that of ultraviolet light is non-ionizing radiation because its energy per quantum is lower than what is needed to remove an electron from an atom. However, the ability to ionize is not required in order to cause disturbances in electronics. For example, in silicon, microwaves with wavelength of 1 µm are energetic enough to excite electrons from valence band to conduction band. Electrically neutral neutrons are also one source of non-ionizing radiation because of their inability to cause ionization directly. In addition, some part of the energy loss of directly ionizing particle radiation is due to non-ionizing processes.

Particles may also interact via Coulomb scattering with the target nuclei causing changes in the motion of both the incident particle and the target nucleus. This interaction is known as the nuclear stopping and it is always screened by the electron cloud of the atom. The nucleus removed from its lattice site, known as a recoil, may in turn cause ionization in the material. Despite the name, nuclear stopping is not due to nuclear forces as it is an electromagnetic interaction. Nuclear stopping becomes more dominant at lower energies as the velocity of the incident particle becomes lower than the velocity of the electrons. Nuclear stopping is mainly notable

for heavy ions.

Electric fields, for example one created by a nucleus, deflect charged incident particles causing them to accelerate (or decelerate), and this change of velocity occasionally leads to an emission of a photon. This process, known as bremsstrahlung or radiative stopping, takes place at high energies and is mostly relevant for electrons [11].

The energy loss of particles per unit path length in certain medium is called the stopping power, $-dE/dx$. The stopping power, also known as the stopping force [12], is the sum of the three effects described below:

$$\frac{dE}{dx} = \frac{dE}{dx}_{(electronic)} + \frac{dE}{dx}_{(nuclear)} + \frac{dE}{dx}_{(radiative)} \tag{1}$$

The electronic stopping power of charged particles is usually quantified experimentally but a theoretical formula derived by Hans Bethe is widely used:

$$-\frac{dE}{dx} = \frac{4\pi z^2 N_A Z\rho}{m_e c^2 \beta^2 A}\left(\frac{e^2}{4\pi\epsilon_0}\right)^2 \cdot \left[\ln\left(\frac{2m_e c^2\beta^2}{I}\right) - \ln\left(1-\beta^2\right) - \beta^2\right] \tag{2}$$

where $v = \beta c$ is the velocity of the particle, c is the speed of light in vacuum, z is its electric charge number, e is the elementary charge, Z, A and ρ are the atomic number, atomic weight and density of the stopping material, N_A is the Avogadro's number and m_e is the electron mass. The parameter I is the mean excitation potential of the target material which is usually regarded as an empirical constant [13]. Also other theoretical formulas, e.g. by Niels Bohr, for the electronic stopping power exist [14]. Semi-empirical formulas and computer codes, such as the SRIM code [15] by James Ziegler, are often used to obtain the electronic stopping power. The results from all these different methods may vary from the experimental results, especially with heavier particles, as shown in ref. [16].

Figure 1 shows how alphas and electrons travel in a medium. Since interactions occur mostly with atomic electrons, the primary electrons' paths show a lot of rapid changes in the direction. The direction of motion of the much heavier alpha particle does not change much during its travel. Figure 2 shows qualitatively the relative transmitted intensities of an alpha and electron beam as a function on material thickness. Compared to heavier particles, light electrons scatter easily and path lengths may differ largely from the average penetration depth. This leads to heavier particles having much more definite range compared to electrons, as demonstrated in the figure.

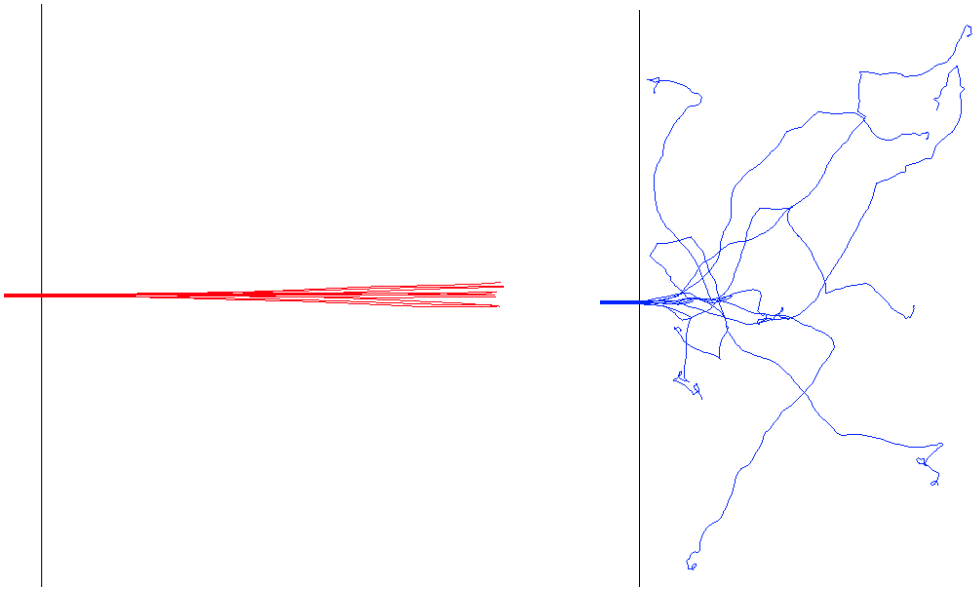

(a) (b)

Figure 1: Paths of (a) 40 MeV alpha particles and (b) 500 keV electrons in silicon, simulated with Geant4.

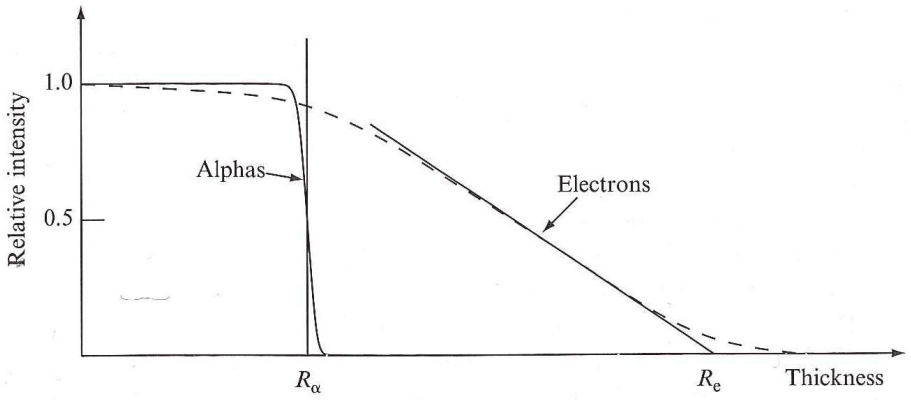

Figure 2: Relative transmitted intensity of alpha and electron beams as a function of the thickness of the medium [17].

The Bragg curve, shown in figure 3, illustrates the stopping power of charged particles as a function of distance traveled in water. The distinct peak near the end of the Bragg curve is known as the Bragg peak. The Bragg peak is the point where the stopping power is at its maximum and it takes place right before the particle is stopped. It should be mentioned, that particle stopping is a statistical process. For a certain traveled distance, the number of ionized atoms and the energy lost per collision as well as the total energy loss varies. The variation of the energy loss is known as straggling [17].

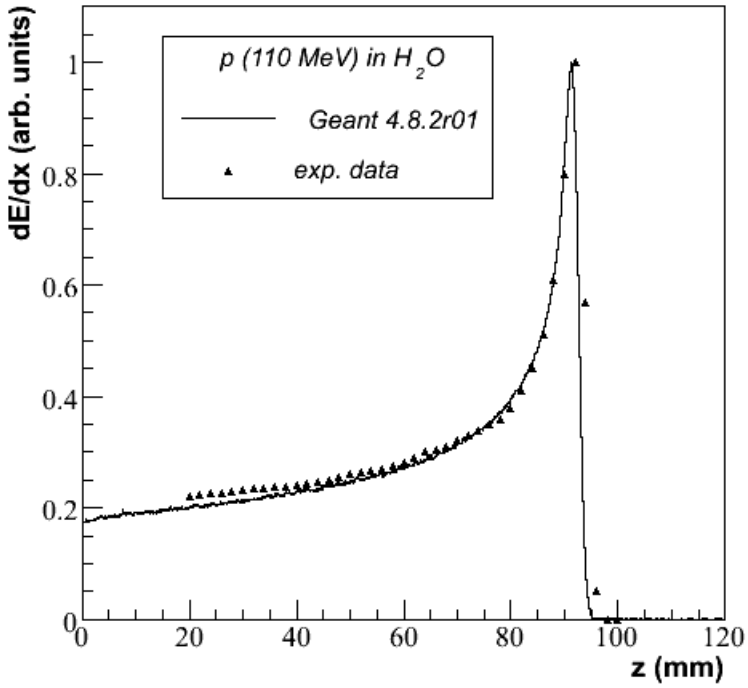

Figure 3: Energy loss of protons in water [18]

In medical and space community, linear energy transfer (LET) is the quantity which describes the energy deposition of a charged particle in material, such as human tissue or an electronic component. The slight difference between the stopping power and LET is that the energy lost by the particle, described by the stopping power, may not be fully deposited into the studied volume. Energy might exit the volume in the form of bremsstrahlung or recoiling particles, e.g. delta electrons. As LET and stopping power are almost equal for large target volumes, LET is often approximated by

$$LET \approx \frac{dE}{dx}_{(electronic)} + \frac{dE}{dx}_{(nuclear)}, \tag{3}$$

or even

$$LET \approx \frac{dE}{dx}_{(electronic)}. \tag{4}$$

The LET as well as the stopping power is typically given in units of MeV/mg/cm^2. The LET of krypton in silicon as a function of energy is shown in figure 4. It can be seen that same values for the LET occur in the low and high energy regime. In single-event upset rate predictions, particles with the same LET have often been considered to have the same effect when disregarding the differences in penetration range between the low energy and high energy ion. The validity and applicability of the LET as a metric for single-event effect rate prediction has, however, been questioned [19]. This will be discussed in more detail in section 4.3.

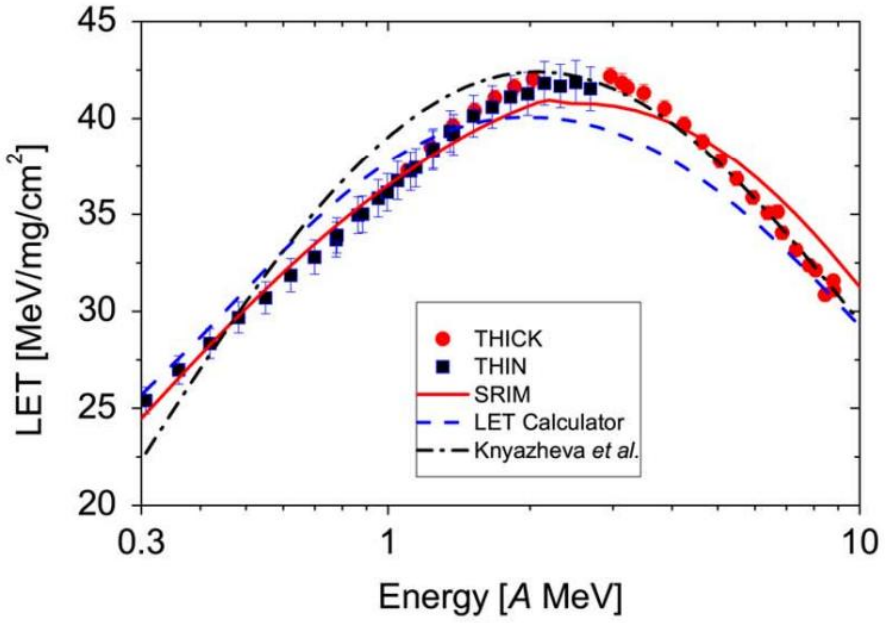

Figure 4: Linear energy transfer of krypton in silicon as a function of energy [16].

The mechanisms how the electromagnetic radiation, gamma rays and x-rays, interact with matter are different from those of particle radiation. The three mechanisms of energy loss for photons are photoelectric absorption, Compton scattering and pair production. Each of these mechanisms have a region of dominance with respect to the energy of the radiation.

In photoelectric absorption, also known as the photoelectric effect, a photon loses all of its energy by releasing an electron, known as the photoelectron. This is the most significant effect for low-energy photons.

In Compton scattering, named after its discoverer Arthur Compton, a photon interacts with a nearly free electron. Part of the incoming photon's energy is transferred to the scattering electron, resulting in a less energetic photon.

The third interaction mechanism is pair production where the photon disappears and creates an electron–positron pair. This process is important in the high energy region and it has a threshold energy of $2m_e c^2$ or 1.022 MeV, the rest mass energy of the created particles. Figure 5 shows the regions of dominance for these three processes described above. This work will, however, focus on particle interactions.

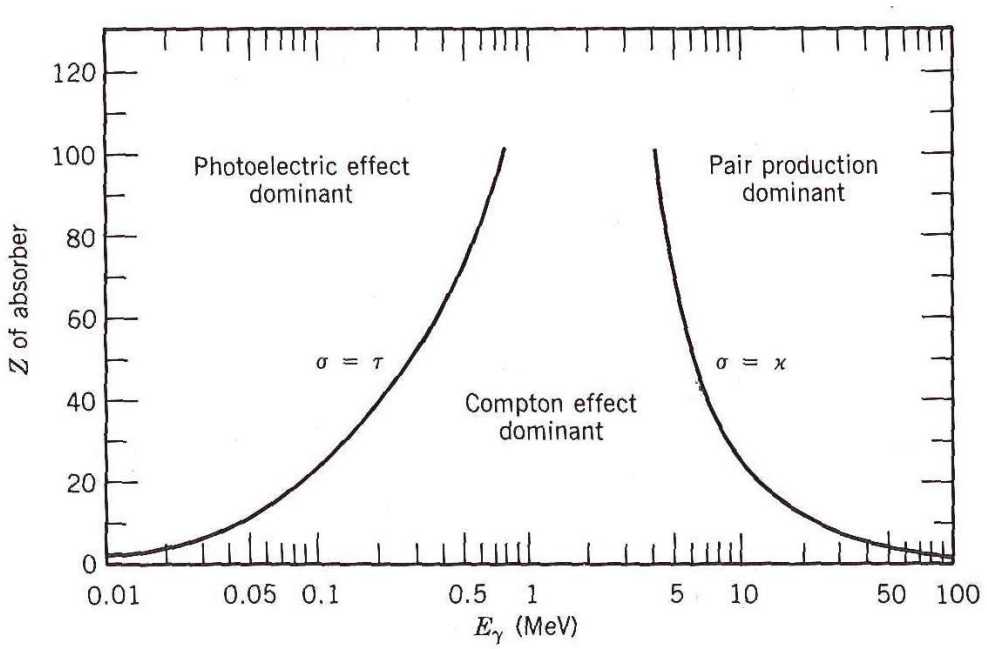

Figure 5: The three gamma ray interaction mechanisms and their regions of dominance [13].

2.1.2 Nuclear interactions

Apart from electronic interactions, so called hadronic particles – protons, neutrons, π mesons and nuclei – may also interact with the target via the strong force in nuclear interactions. The strong force is what holds nucleons together in a nucleus and it has a significantly shorter range than the electromagnetic force. For charged particles this means that they must have enough kinetic energy to overcome the Coulomb repulsion, known as the Coulomb barrier, before they can enter a nucleus and set off a nuclear interaction. The Coulomb barrier is defined by:

$$V = \frac{1.44 Z_i Z_T \text{ MeV} \cdot \text{fm}}{R_i + R_T} = \frac{1.44 Z_i Z_T \text{ MeV} \cdot \text{fm}}{R_0 (A_i^{1/3} + A_T^{1/3})} = \frac{1.2 Z_i Z_T \text{ MeV}}{A_i^{1/3} + A_T^{1/3}}, \tag{5}$$

where $R_0 = 1.2$ fm, Z_i and Z_T are the charge numbers of the incoming and the target nuclei, respectively, A_i and A_T are their mass numbers and R_i and R_T are their radii [20]. In the case of a compound reaction, since the incoming particle has linear momentum, the outgoing particle must also have linear momentum due to conversation of linear momentum. Thus, the kinetic energy of the projectile must exceed the Coulomb barrier threshold kinetic energy K_{CBT}:

$$K_{CBT} = V\left(1 + \frac{m_i}{m_T}\right) = \frac{1.2 Z_i Z_T \text{ MeV}}{A_i^{1/3} + A_T^{1/3}}\left(1 + \frac{m_i}{m_T}\right) = \frac{1.2 Z_i Z_T \text{ MeV}}{A_i^{1/3} + A_T^{1/3}}\left(1 + \frac{A_i}{A_T}\right).$$

Nuclear interactions are classified in many ways, one being the separation into elastic and inelastic processes. In elastic nuclear collisions, some fraction of the projectile's kinetic energy is transferred to kinetic energy of the target atom but no excitation or fragmentation takes place. In inelastic collisions, some part of the kinetic energy of the primary particle goes into the excitation or fragmentation of the target nucleus. No single theory explaining the reaction dynamics of heavy ion collisions exists and the complementary use of several theories or models compassing different energy ranges and particle species is often necessary [21]. At Coulomb barrier energies (several MeV/nucleon), one has to deal with compound nucleus formation and deep inelastic scattering in terms of hadrons and their resonances. At high energies, quark and gluon degrees of freedom are to be used [22].

Energetic neutrons may be captured by nuclei and the resulting daughter nuclei are often unstable leading to radioactive decay. After neutron capture, an excited nucleus may decay by emitting a gamma ray or by fragmenting into smaller particles. The fragmentation of a nucleus into parts, e.g. two heavy parts and some neutrons and photons, is called fission. The opposite reaction, where two or more particles are combined into one nucleus is called fusion. Nuclear reactions are stochastic, non-deterministic, events which are characterized by their specific probability known as *cross-section*. Nuclear cross-sections depend on the target nucleus, the incoming particle and its energy. Figure 6 shows the neutron capture cross-section for ^{10}B and ^{197}Au [23]. As can be seen in the figure, the neutron capture cross-section of ^{10}B is generally higher compared to that of ^{197}Au. But at certain energies, the neutron capture cross-section of ^{197}Au varies rapidly due to so-called *resonance effects*, which are not discussed in this work.

The energy balance in nuclear reactions is defined by difference in binding energies between the final and the initial reaction products. Fusion of ^{2}H (deuterium) and ^{3}He results in the formation of ^{4}He and a proton. Since the binding energy per nucleon of ^{4}He is much higher than that of either of the initial products, the difference in masses is released in the form of energy. In other words, the sum of the masses of the initial products are lower than that of the final products. This difference in masses (or energies) is known as the Q value, and a reaction with a positive Q value is called an exothermic reaction, where energy is released [17]. The figure 7 shows the bind-

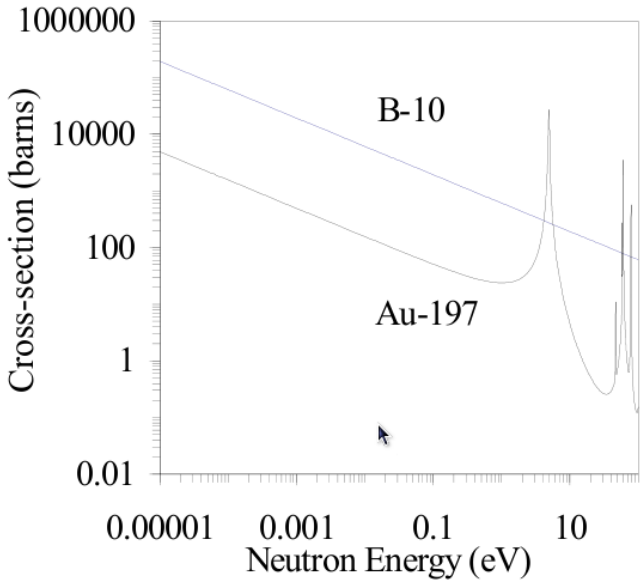

Figure 6: Neutron capture cross-section for ^{10}B and ^{197}Au as a function of neutron energy [23].

ing energies per atomic mass units as a function of mass number. The knowledge of nuclear reactions is important in the SEE context because they can add a significant contribution to the energy deposition spectrum in addition to the conventional direct ionization. For example, fission fragments after a neutron capture of ^{235}U may cause high local ionization.

Figure 8 shows how different types of radiation lose their energy in ionization with respect to the distance traveled in matter. Cobalt-60 is a gamma emitter. As opposed to charged particles, such as electrons or protons, photons and neutrons do not carry electric charge and the intensity of a photon or neutron beam decays exponentially as a result of multiple scatterings and absorptions. This leads to a monotonous, decreasing behaviour for their stopping power.

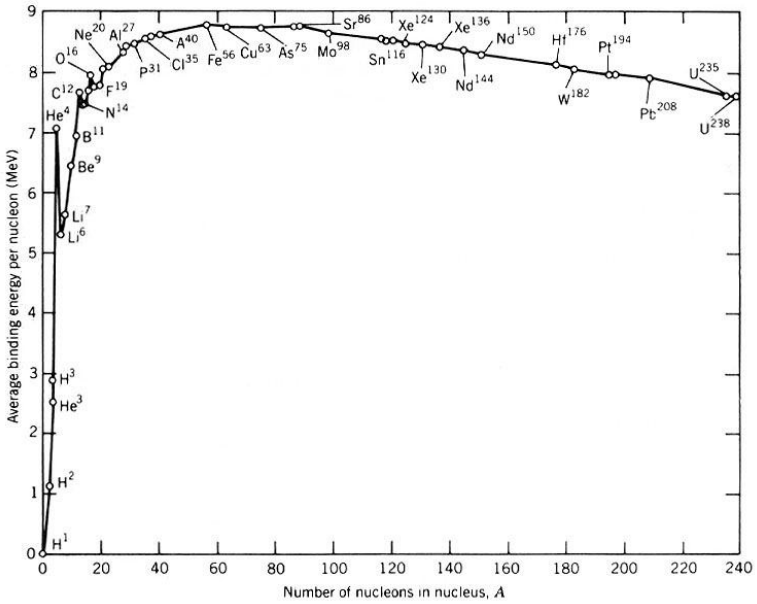

Figure 7: Nuclear binding energy per atomic mass unit as a function of mass number [24].

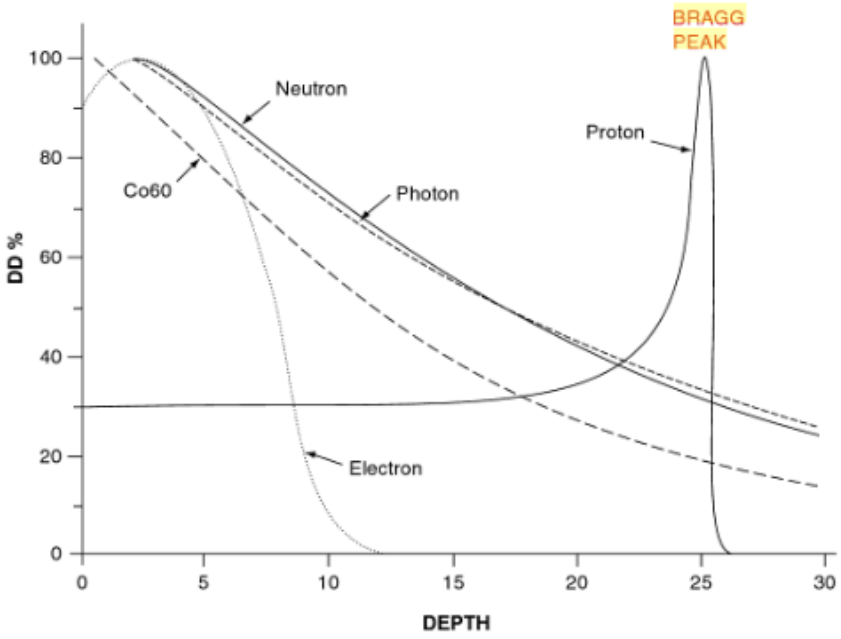

Figure 8: Distributed dose of different radiation types as a function of depth in a medium[25].

3 Radiation sources in space

Radiation in space is a major concern for the proper operation of spacecraft electronics as well as for the safety of the humans on manned spaceflights. The knowledge of the radiation environments in space and the induced effects is crucial for designing reliable yet cost-effective spacecraft systems. The main sources of external radiation in space are divided into three categories: Galactic cosmic rays, solar wind particles and radiation belts [2].

3.1 Solar particles

The Sun emits vast amounts of electromagnetic and particle radiation. The activity of the Sun varies in cycles between a solar maximum and solar minimum, and this is known as the solar cycle or the sunspot cycle. The average time between two minima is 10.6 years and between two maxima 11 years [26]. The solar activity is estimated by counting the number of sunspots visible on the Sun, the maximum of sunspots signifying the solar maximum. Sunspots are dark and cold areas on the Sun's surface where heat transport is blocked by the strong magnetic field [27]. The presence of sunspots manifests intense magnetic activity in the Sun.

The solar wind is an outflow of particles constantly ejected from the Sun's corona with a flux that varies with the solar activity. The solar wind consists of energized, charged particles, mainly electrons and protons [27]. The interaction between the solar wind and the magnetic field of a planet is responsible for the overall shape of the planet's magnetosphere.

The solar wind and the rather unpredictable solar energetic particle (SEP) events, such as the solar flare and coronal mass ejection, are a predominant source of radiation in the solar system. The solar flares are sudden bursts of electromagnetic radiation accompanied by energetic ions and electrons. The energy spectrum of electromagnetic radiation in solar flares ranges from long radio waves to short x-rays and gamma radiation. The solar flares are caused by magnetic reconnection between the loops of magnetic field lines. The reconnection phenomenon results in an arrangement which stores less energy and the released energy is responsible for the particle acceleration [27]. Solar flares are difficult to predict but are more frequent during the active phase of the Sun.

Coronal mass ejections (CME) are balloon-shaped bursts of plasma from the Sun's corona. Huge masses, up to 10^{13} kg [28], of highly energetic charged particles can be ejected into the interplanetary medium at high speeds of the order of hundreds of km/s [27]. The collision of a CME with a planet may cause temporary disturbances in the magnetosphere, also known as magnetic storms.

3.2 Radiation belts

Charged particles trapped in the Earth's magnetosphere compose a high radiation field in the vicinity of the Earth. These trapped particles create a torus-shaped formation and are therefore also known as the radiation belts. The radiation belts around the Earth are also known as Van Allen Belts after James van Allen, who was one of the scientists involved in the early research of the radiation belts. The Van Allen belts were first discovered in 1958 when a Geiger–Muller tube on the Explorer 1 satellite become so highly saturated that it completely stopped generating pulses.

Currently, we don't have a complete understanding of the sources of the particles in the radiation belts but origins are considered to include the solar wind, low-energy galactic cosmic rays, electrons from the ionosphere and the decay products of neutrons (namely protons and electrons) resulting from collisions of interplanetary cosmic rays with atmospheric atoms (cosmic ray albedo neutron decay, CRAND) [29]. Particle trapping takes place because of the Lorentz force exerted on charged particles by the magnetic field of the Earth, restraining particles and keeping them contained within defined regions around the Earth.

The Earth's radiation belts are divided into two regions, referred to as the inner and the outer belt. An illustration of the Earth's radiation belts is shown in figure 9. The inner belt is mainly populated by protons with energies ranging from tens of keV to hundreds of MeV, and is often called the proton belt. The altitude of the inner radiation belt ranges from 100 to 10 000 km. The outer belt, also known as the electron belt, extends from an altitude of three to ten Earth radii and is populated mainly by electrons with energies exceeding tens of MeV. There are also some heavy ions trapped in the Earth's magnetic field but with intensities lower than those of protons and electrons. The energies of these heavy ions are typically of some tens of MeV/nucleon so even the thinnest shielding will be able to stop them [10].

Other planets with strong magnetic fields are also expected to be surrounded by radiation belts. Of the planets in the solar system, Jupiter has the most intense radiation belt. Also Saturn, Uranus Neptune and Mercury are known to have radiation belts but measurements indicate that their trapped radiation zones don't pose a threat to spacecraft systems [29]. Venus and Mars cannot support radiation trapping due to the weakness or a complete lack of internal magnetic fields.

3.2.1 South Atlantic Anomaly

Above the South Atlantic ocean the magnetic field of the Earth is weaker than elsewhere because the magnetic axis of the Earth is tilted and offset with respect to the rotation axis [31]. Weakened magnetic field allows incoming charged particles from outer space to enter deeper into the atmosphere. This creates the effect called South Atlantic Anomaly (SAA) which is of great significance to low-altitude spacecraft and must be considered in radiation protection. Figure 10 shows how the X-ray detectors

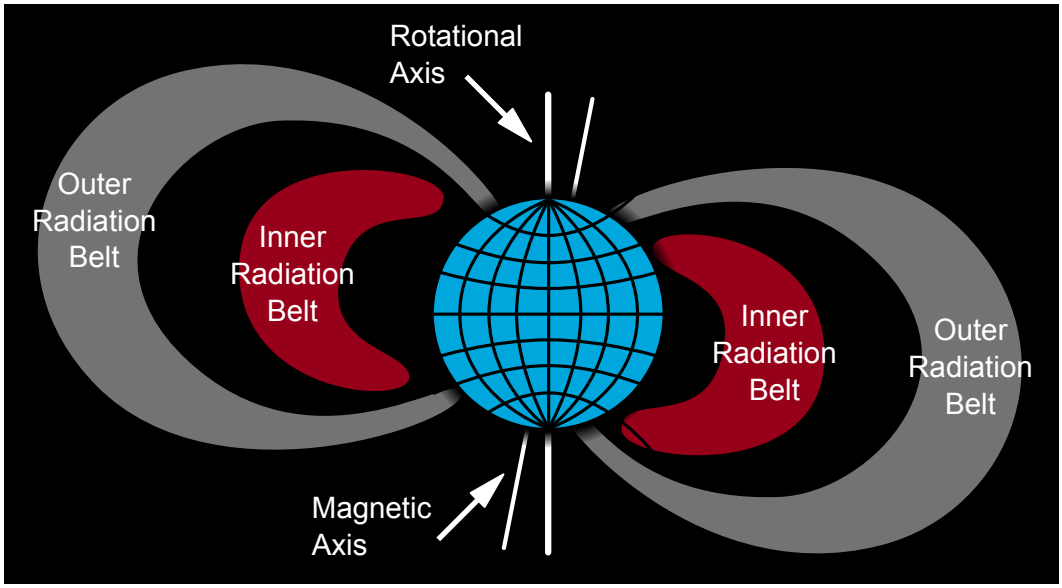

Figure 9: Van Allen belts [30].

on the ROSAT satellite were affected by the SAA.

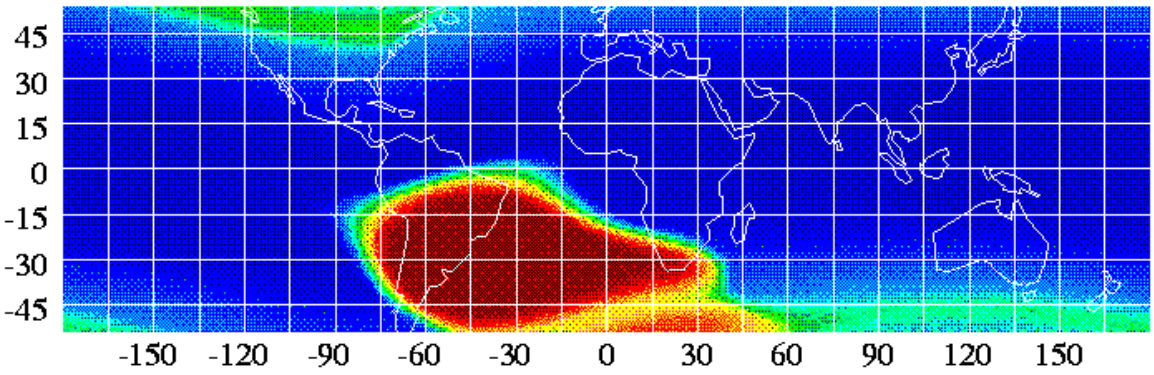

Figure 10: The South Atlantic Anomaly [32].

3.3 Galactic Cosmic Rays

Galactic cosmic rays (GCR) are subatomic particles from outside of the solar system traveling in space carrying large amounts of kinetic energy. The discovery of GCR dates back to the early 1900's when Victor Hess devised his experiment and put an electroscope in a balloon to get it away from the natural radiation of the Earth [29]. To his surprise, he noticed that the radiation levels actually rose as the balloon was

ascending, and so he was able to conclude that the source of radiation must come from outer space. Also, as the intensity of the radiation did not vary depending on the time of day it was concluded that the radiation was not of solar origin.

GCR are ionized nuclei constantly bombarding the Earth's atmosphere. Roughly 83% of them are protons, 13% alpha particles, 3% electrons and the rest are heavier nuclei [27]. Cosmic rays are mostly relativistic, which means that their energies are comparable to their rest mass (for proton, the rest mass $\approx$ 938 MeV/c^2) [33]. Occasionally GCR have such high energies that it is unclear what kind of physical process could have accelerated them.

The origin of GCR is unknown and a matter of scientific debate, but most of them come from inside of our galaxy [33]. Some of the GCR have such high energies that it has been deduced, by the shape of their trajectories, that they might be of extragalactic origin. Figures 11 and 12 show the energy spectrum for cosmic rays and the relative abundances of the heavy ions in cosmic rays.

GCR form a constant background of high penetration radiation which is hard to protect against. In fact, shielding may even make the situation worse by decreasing the energy but increasing the LET.

The Earth's magnetic field offers efficient protection by deflecting the trajectories of GCR. Cosmic rays that penetrate into the Earth's atmosphere collide with the air molecules leading to showers of secondary particles, such as electrons, pions and muons. Despite the magnetic field and the atmosphere, some particles are able to get to ground level. These particles are mainly muons, electrons and neutrons from collisions between cosmic rays and nitrogen or oxygen nuclei in the atmosphere. Occasionally, these particles can cause bursts of charge in semiconductor devices and cause errors. For example, the release of an highly ionizing alpha particle in the ^{28}Si(n,n'α)^{24}Mg reaction is one hazardous example which can result in a non-destructive device malfunction [34].

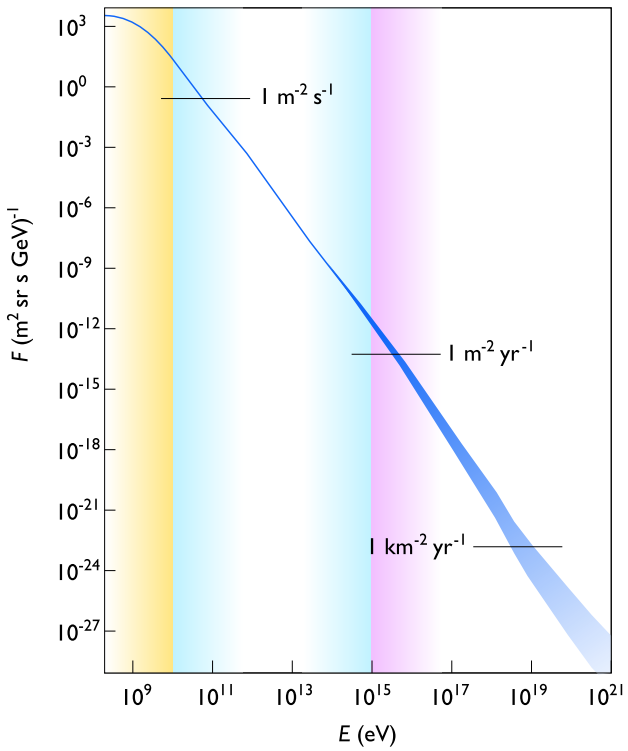

Figure 11: The energy spectrum for cosmic rays [35].

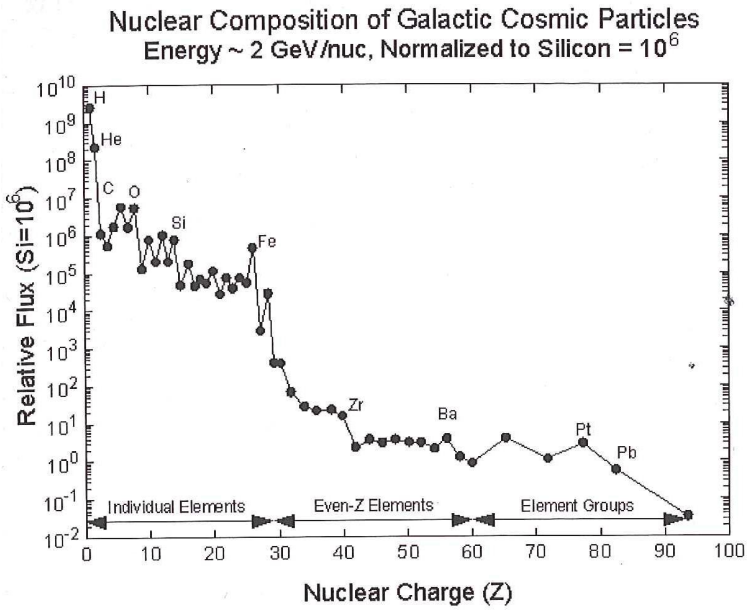

Figure 12: Relative abundances of galactic cosmic ray ions in interplanetary space [11].

4 Radiation effects

Ionizing radiation can cause DNA mutation in living organisms resulting in both short-term and long-term damage. The analyzes of historical solar particle events (SPE) have shown that lethal doses could have been delivered to astronauts [36]. For the safety of humans spending time in space, minimizing the radiation-related health risks is important but beyond the scope of this work.

The possible radiation effects in electronic devices can be divided into three main categories: Total ionizing dose, displacement damage and single-event effects. Total ionizing dose occurs as a cumulative effect after a build-up of trapped charge in a device which can lead to parametric shifts and functional failures. The energy loss of incident ions resulting in nuclei being displaced from their normal lattice position is known as displacement damage. Displacement damage is also a cumulative effect and may lead to degradation of device characteristics. Single-event effects, however, are effects resulting from a passage of a single energetic particle creating a cloud of charge in the device.

4.1 Total Ionizing Dose

Total ionizing dose (TID) effects are due to the progressive build-up of defects and trapped charge in semiconductor devices. TID effects are usually observed as increased leakage currents. The shift of the threshold voltage of an NMOS transistor may lead to a permanent on-state which cannot be turned off [37]. TID reduces the performance of a system gradually until the device fails to function.

4.2 Displacement Damage

Most of the energy lost by energetic charged particles in a medium is lost to atomic electrons via ionization. However, when incident particles interact with the nuclei of the material the nuclei may receive enough kinetic energy to be displaced from their lattice site. A displaced nucleus leaves behind an empty vacancy and may, depending on its energy and the temperature of the material, recombine with a vacancy or move into a non-lattice position creating a long-term crystal defect known as an interstitial [38]. If the recoil has enough energy it can also displace other nuclei and trigger a cascade of displaced atoms.

The inflicted displacement damage depends on the primary particle type and energy and on the target material characteristics. The defects in irradiated materials created by electrons or photons are often far apart and point-like. Defects produced close together, however, may form disordered regions, also known as defect clusters. These disordered regions can be created when an energetic, displaced nucleus dislodges many other nearby nuclei [39]. Displacement defects will in time reorder to

more stable configurations, an effect known as annealing. The reordering process is also temperature dependent and can be enhanced by heating the material. Heating is typically used to reduce the amount of defects, but can, in fact, in some cases lead to more defects [38].

The created defects may alter the material properties, such as the electronic band gap structure in semiconductors. New, allowed energy levels in the band gap change the electrical and optical properties of the material, and potentially alter the operation of a device. In bipolar-junction transistors, displacement damage can increase the carrier recombination in forward biased junction, thus reducing the current gain of the transistor [40].

4.3 Single-event Effects

Single-event effects (SEE) are any kind of errors in a device caused by the energy deposition of a single energetic particle crossing its sensitive area. Some of these errors are classified as *soft* errors, which induce temporary and reversible effects in the device. This may be loss of information, such as an inversion in a stored bit, which can be recovered by rewriting the data. *Hard* errors, however, lead to permanent physical damage, such as a rupture of the gate oxide in a MOSFET.

The number of acronyms for the variety of SEEs is plentiful. The soft errors include SEU (Single Event Upset), MBU (Multiple Bit Upset), SET (Single Event Transient) and SEFI (Single Event Functional Interrupt), while some of the hard errors are known as SEGR (Single Event Gate Rupture), SHE (Single Hard Error), SEL (Single Event Latchup), SEB (Single Event Burnout), SES (Single Event Snapback) and SEDR (Single Event Dielectric Rupture) [41]. Of these, only SEU will be discussed in more detail.

4.3.1 Single-event upsets (SEU)

Single-event upsets are soft errors, meaning that the integrated circuit can be recovered to a fully functional state. SEUs usually mean a change in the logic state of a memory cell which can be corrected by rewriting the data to the cell. The probability for a device to be upset is known as the SEU cross-section, and it is an important factor in predicting how a device will function in a radiation environment. The SEU cross-section is traditionally considered to depend mainly on the particle LET, increasing with increasing LET. The SEU cross-section can be given in number of cm^2/bit or cm^2/device. The SEU cross-section relates to an actual area because at high LET values the SEU cross-section usually saturates to a certain value and each particle crossing the device is considered to cause an upset, thus outlining a projected area.

The mechanism behind SEUs is the following: a penetrating particle deposits en-

ergy into a semiconductor and generates electron–hole pairs (= carriers) which are then transported within the semiconductor. Before the electron–hole pairs have time to recombine, a fraction of them is separated by the electric field near a p–n junction of the semiconductor and collected at the nearby device contact. If the collected charge exceeds the critical threshold, an SEU occurs. Reverse-biased p–n-junctions are the most sensitive regions to SEUs because of their large depletion region and strong electric field [42] [43].

In order to explain how an SEU occurs in a static random access memory (SRAM), the structure of SRAM should be explained. SRAM is a semiconductor memory which retains the stored information as long as the supply voltage is applied. One SRAM cell, shown in figure 13, which stores the information of one bit typically consists of two inverters (M1 & M2 and M3 & M4 in figure), and two access transistors (M5 and M6 in figure 13). Both inverters are complementary metal-oxide-semiconductor (CMOS) inverters which are pairs of p-type and n-type metal-oxide-semiconductor- field-effect-transistors (MOSFETs). Briefly, an n-type MOSFET (NMOS) is in conducting state ("on") when a positive gate voltage is applied whereas for the p-type (PMOS) the case is the opposite. Access transistors are typically NMOS transistors disconnecting the cell from the bit-lines (BL and $\bar{\text{B}}\text{L}$ in figure 13) when word-line (WL) is set to 0.

When the value of the SRAM cell is read the word-line is set to logical 1 in order to open the access transistors. Consequently, the stored value is transferred from the first inverter to the bit-line and the complement of the stored value from the other inverter to the complement bit-line. Write operation begins by setting the value to be stored to the bit-line and its complement to the complement bit-line, and then by asserting the word-line. For example, when logical 1 is set to bit-line and logical 0 to complement bit-line and the word-line is opened, the bit-line values are connected to the inverters switching transistors M1 and M4 "on" and transistors M2 and M3 "off". Thus, the logical 1 from the V_{DD} is stored at node Q and logical 0 at $\bar{\text{Q}}$ even after the access transistors are switched off.

Now, let us consider an ion strike and a consequent SEU. The most radiation sensitive transistors are the off-state transistors. If the stored value is logical 1 and the ion strikes near the off-state NMOS (M3), it will be temporarily switched "on" lowering the output of the inverter. If the PMOS of the same inverter (M4) cannot supply enough current to maintain the output of the inverter the state of the second inverter (M1 & M2) will be changed consequently switching the stored value of the SRAM to 0. Same principle applies if the stored value is 0, in which case the sensitive transistors are the opposite (M1 and M4).

SEUs in space are mostly attributed to heavy ions outside the Earth's radiation belts originating from cosmic rays or solar flares. However, many satellites reside in geostationary orbits in the altitudes of 30 000 – 50 000 kilometers where also protons of the proton radiation belt cause SEUs, mostly via indirect ionization. Roughly, 1 in

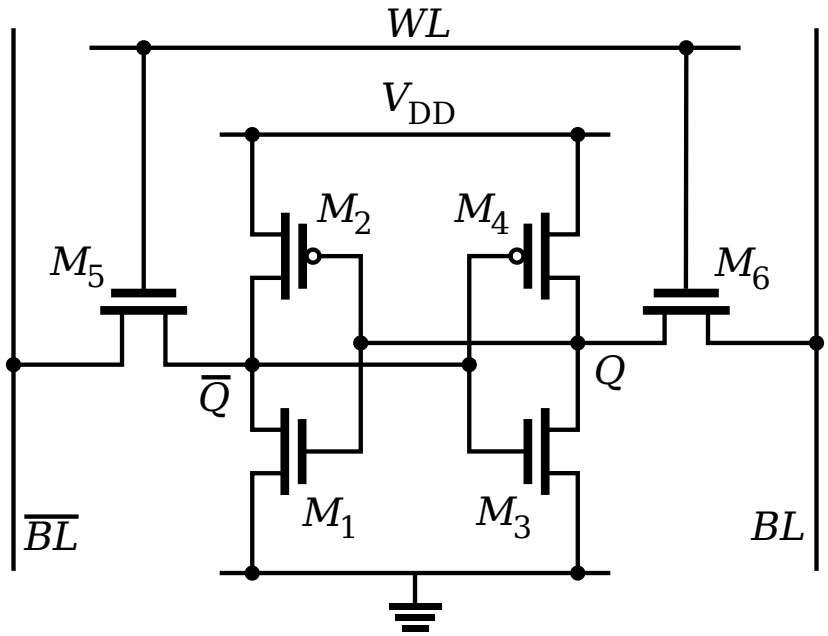

Figure 13: A six-transistor SRAM cell [44].

10^5 protons induces a nuclear reaction in silicon which may be capable of producing an SEU. Depending on the proton upset cross-section of the device, this may be significant as the flux of protons with kinetic energies above 30 MeV in the proton belt is about 10^7–10^9 protons/cm^2/day [45].

As cosmic rays interact with the nuclei in our atmosphere, a significant amount (10 n/cm^2/h) of neutrons, known as atmospheric neutrons, reach sea level. Neutrons cause SEUs via several different mechanisms including scattering, absorption and spallation as well as alpha emissions after a neutron capture. Predictions of device failures in electronics at aircraft altitudes were published already in 1984 [46]. In a paper published in 1995 [47] it was shown, with the help of more than 1000 hours of flight data, that non-radiation-hardened memories on airplane altitudes suffer from errors due to cosmic rays. In addition, due to the raised awareness of the possible health risks from exposure to cosmic rays, the assessment of the in-flight radiation exposure of air crew became mandatory for airlines in the European Union in the year 2000 [48].

For long, the potential for ground level device failures due to cosmic rays received very little public recognition on chip manufacturer's side [7]. Some studies concerning ground level effects due to cosmic rays were kept proprietary. However, in 1994 IBM published a paper in which they review the research and experimental work carried out between years 1978 and 1994 in evaluating the effects of cosmic rays on terrestrial electronics [8]. In ref [7], the authors present various examples of errors

induced by cosmic rays in the computers of that time, implicating that cooperation between the community behind these studies and the designers of microelectronics and commercial electronics manufacturers would be advantageous.

4.4 Radiation hardening

The radiation effects of devices can be decreased with a number of approaches. Describing these methods in detail is outside of the scope of this work and they will only be explained briefly. The names of the radiation hardening techniques vary between sources and the used techniques may not always fall strictly into one category, i.e., some overlapping exists.

One approach to make circuits radiation hard is known as *hardening by process*, in which the fabrication process of a device is optimized to make it less sensitive to radiation. Hardening by process encompasses, for example, careful selection of materials, thermal treatments and modification of doping profiles in devices and substrates, [49]. Hardening by process is not very attractive for the electronics industry since the markets for radiation hard components are small. Thus, commercial-off-the-shelf (COTS) components are often used and radiation hardness is obtained by other means.

Hardening by design is an approach in which the layout of a circuit is designed with radiation hardness in mind. Radiation hardness is obtained, for example, by choosing transistors known to have rad-hard qualities or by adding certain circuit functions. This approach makes it possible to use commercial technologies instead of custom technologies which are often expensive and capacity-wise inferior.

Hardening by design can mitigate TID and single-event effects and usually leads to increased circuit areas and decreased operating speed [49]. One example of mitigating SEEs by increasing the critical charge of a circuit is achieved by adding feedback resistors between the inverters in an SRAM memory. This slows down the operation and gives the struck inverter more time to recover before the value of the cell is changed. The feedback resistors can also be replaced by gated resistors, which in fact are transistors conducting only during write operations.

System level hardening mainly includes two different kind of approaches. One is obtained by redundancy, which means that the output of a circuit actually depends on several copies and the output is determined by a voting system. In addition, the redundant circuits can be placed far from each other in order to prevent a single ion from upsetting more than one of them. The drawback with this approach is obviously the increased size and power consumption.

Another approach which falls into the category of system level hardening is the use of architecture and algorithms which are able to detect and correct errors. Error Detection and Correction (EDAC) schemes, such as a Hamming code, are effective in detecting and correcting single bit flips. This is achieved by adding redundancy

to each word which can used to check the consistency. Most of the algorithms in use are able to correct one and detect two errors in a single word. Current algorithms correcting more than one error, however, lead to increased complexity in a way which is mostly unfeasible. By associating neighboring bits to different words, a technique known as interleaving, one can hinder the occurrence of multiple errors in a single word effectively. An example of interleaving is shown in figure 14.

The trend of increasing the density and speed of devices often leads to increased radiation sensitivity. Typically, radiation sensitivity of devices has not been a major concern of commercial manufactures. This might change, however, if highly scaled devices start to become sensitive to particles which are frequently observed at sea level.

Original sentence:

$$\boxed{A_1B_1C_1D_1}\ \boxed{A_2B_2C_2D_2}\ \boxed{A_3B_3C_3D_3}\ \boxed{A_4B_4C_4D_4}$$

Interleaved sentence:

$$\boxed{A_1A_2A_3A_4}\ \boxed{B_1B_2B_3B_4}\ \boxed{C_1C_2C_3C_4}\ \boxed{D_1D_2D_3D_4}$$

Interleaved sentence after an ion strike:

$$\boxed{A_1A_2A_3A_4}\ \boxed{B_1\,\_\_\_\_}\ \boxed{\_\_C_2C_3C_4}\ \boxed{D_1D_2D_3D_4}$$

Decoded sentence:

$$\boxed{A_1B_1\,\_\_D_1}\ \boxed{A_2\,\_\_C_2D_2}\ \boxed{A_3\,\_\_C_3D_3}\ \boxed{A_4\,\_\_C_4D_4}$$

Figure 14: Interleaving can decrease the probability of multiple-bit upsets. Single-bit upsets within a byte can be efficiently recovered.

5 SEU rate prediction

The relevance of predicting the rate at which SEUs occur in spaceborne electronics became apparent in the late 1970s after the first discoveries of radiation-induced errors. Many concepts from the early error rate prediction models established at that time, as for example in ref. [50] and [51], have remained in use until these days. Traditionally SEUs caused by heavy ions and protons have been estimated separately due to the different nature of the energy deposition leading to upsets. The methods of predicting the SEU rate related to heavy ions have been based on the direct-ionization in terms of LET. Protons, however, have been considered unable to cause SEUs via direct ionization due to their small LET. Instead, the energy depositions of the secondary particles after proton–matter interaction must be considered.

5.1 Traditional heavy ion SEU rate prediction

5.1.1 The chord-length models

The classical SEU rate prediction models, namely the (integral) rectangular parallelepiped models (RPP, IRPP), assume that there is a box-shaped sensitive volume (SV) within a circuit element which will collect the charge generated by the passage of an energetic particle, causing the circuit to upset [52]. The (I)RPP models rely on the assumptions that for a given LET the effect on the device is the same regardless of the particle type or energy, and that an effect will only occur if the deposited energy in the SV exceeds the critical energy E_c. The energy deposition is given simply by

$$E_{dep} = \rho \cdot LET \cdot d \tag{6}$$

with ρ (mg/cm^3) equal to the density of the medium, LET (MeV/mg/cm^2) the linear energy transfer of the particle in the current medium and d (cm) the traversed path length in the sensitive volume.

The relationship between the deposited energy and generated charge is obtained from the average energy required to create one electron–hole pair in certain medium. For silicon, the conversion from energy to charge is obtained from

$$Q\,(\mathrm{pC}) = \frac{e}{3.6\ \mathrm{eV}} \cdot E\,(\mathrm{MeV}) = \frac{1.6022 \cdot 10^{-7}\ \mathrm{pC}}{3.6 \cdot 10^{-6}\ \mathrm{MeV}} \cdot E\,(\mathrm{MeV}) = \frac{E\,(\mathrm{MeV})}{22.5\ \mathrm{MeV/pC}}$$

where e is the elementary charge and 3.6 eV the average energy for e–h pair creation in Silicon. This conversion between energy and charge allows for the interchangeable concepts of a critical energy and critical charge, E_c and Q_c, respectively.

By assuming that the incident particles will move along straight lines in the medium, there is a maximum path-length which a particle can traverse in the sensitive volume. Then, only particles with LET above a certain value, known as the threshold LET, are able to deposit enough energy to upset the circuit.

The SEU rate prediction depends on the energy depositions into the SV in a certain radiation environment. In the (I)RPP models, a single energy deposition is described by the LET and the path-length. Thus, two inputs are needed for the SEU rate prediction: the LET spectrum of the environment and the path-length probability function of the SV. In order to obtain the SEU rate, one must take the integral of the path-length distribution within the sensitive volume with the expected LET spectrum of the environment. The result for the SEU rate is given by the following formula, as obtained by Bradford in ref. [51]:

$$n = \frac{S}{4} \int_{LET_{\text{th}}}^{LET_{\text{max}}} \Phi(\text{LET}) P\left(\frac{E_{th}}{LET \cdot \rho}\right) \mathrm{d}LET \tag{7}$$

where S is the total surface area of the SV, LET_{th} is the threshold LET, LET_{max} is the maximum LET in the environment, $\Phi(LET)$ is the differential LET flux in the environment (particles / $\text{cm}^2 \cdot \text{s} \cdot \text{MeV} \cdot \text{cm}^2$ / g), P is the integral path-length distribution (probability of path-length > $\frac{E_{th}}{LET \cdot \rho}$). The SEU rate formula obtained by Pickel and Blandford in ref. [50] uses integral LET flux and differential path-length distribution and is completely equivalent with (7) [45]. These two methods have been the basic RPP approaches for SEU rate calculations.

The RPP models require values for the critical charge and SV dimensions, which can be deducted from the known device geometry or experimentally. A simple SV shape is chosen because the problem of encountered path-lengths can be treated by a path-length distribution function. For example, SVs with the shape of a cylinder or a hemisphere could be used. However, a parallelepiped SV is usually chosen because of its relation to actual device geometries, such as depletion regions in semiconductors.

In the method explained in ref. [50], the critical charge and the SV dimensions were derived from the device parameters of the memory cell. Another common procedure is to assume a value for the SV depth based on the used technology, and to use the square root of the experimental SEU cross-section at high LET values for the two remaining dimensions. The critical energy (or charge) can be obtained by first determining the threshold LET, for example by irradiating the device with normally incident ions, and using eq. (6) with the assumed SV depth.

The SEU cross-section curves obtained from irradiation tests usually exhibit similar feature as the examples shown in figure 15. The RPP model with only one SV combined with a value for critical charge is equivalent with a SEU cross-section curve with the shape of Heaviside step function. Incoming ions with a fixed angle of incidence on the SV will not exceed the critical charge below certain LET. Above that certain LET, each ion will result in an upset. The difference between the RPP and IRPP models arises from the fact that the measured cross-section curves do not show an abrupt onset but instead exhibit a smooth rise starting from the threshold LET.

In the IRPP model it is assumed that there exists some device-to-device (or SV-to-SV) variation in critical charges or equivalently threshold LETs. Therefore, the

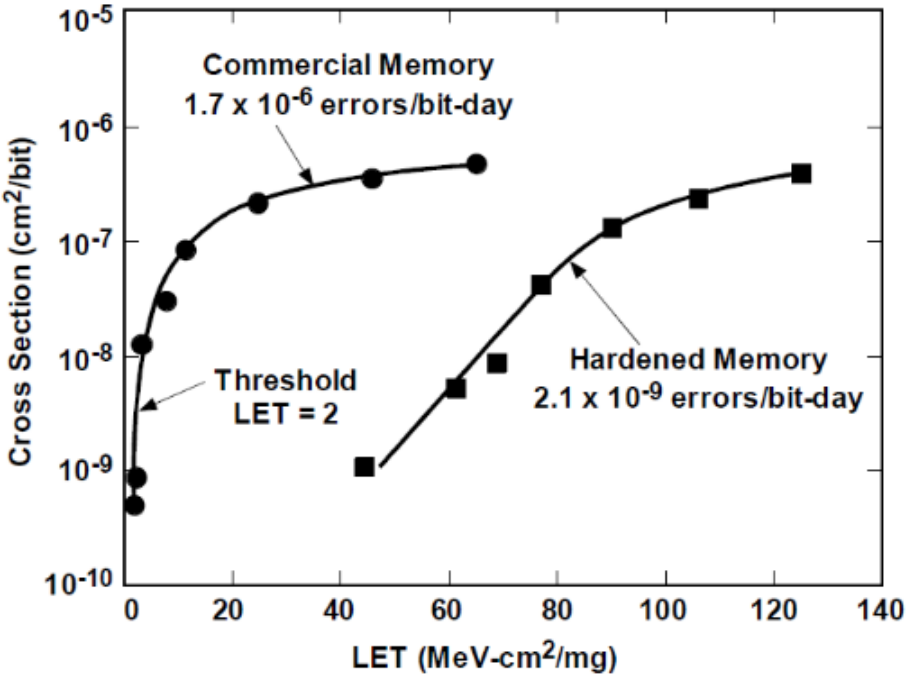

Figure 15: SEU cross-sections of a commercial and a radiation hardened device.

IRPP model consists of several SVs with different critical charges residing in the same radiation environment. The IRPP method, as described in 1986 by Harboe-Sørensen in ref. [53], uses each point on an experimental SEU cross-section curve to determine a critical charge. Each point on the curve corresponds to a fraction of SVs in the device with an unique critical charge. The fraction of SV is obtained from the cross-section value and the corresponding critical charge from the LET by assuming constant SV thickness. The SEU rate is obtained in similar manner as in (7) but the integration is performed in parts with each LET interval corresponding to a certain critical charge. The total rate is then obtained by summing the results from each integration part weighed by the fraction of SVs susceptible to SEUs at the corresponding LET.

An improvement to the IRPP model is obtained by replacing the experimental SEU cross-section with a function and changing the summing operation into an integration. The SEU cross-section curves can usually be described by a Weibull cumulative distribution function, also referred to as the Weibull curve. The IRPP method integrating over an SEU cross-section in the form of a Weibull curve, as suggested in ref. [54], is a standard method of SEU prediction. One widely used implementation is the Cosmic Ray Effects on Micro-Electronics (CREME) code which, among other things, provides the description of radiation environments and SEU rate prediction using the IRPP method.

Figure 16 illustrates the basic idea behind obtaining the SEU rate with the (I)RPP models.

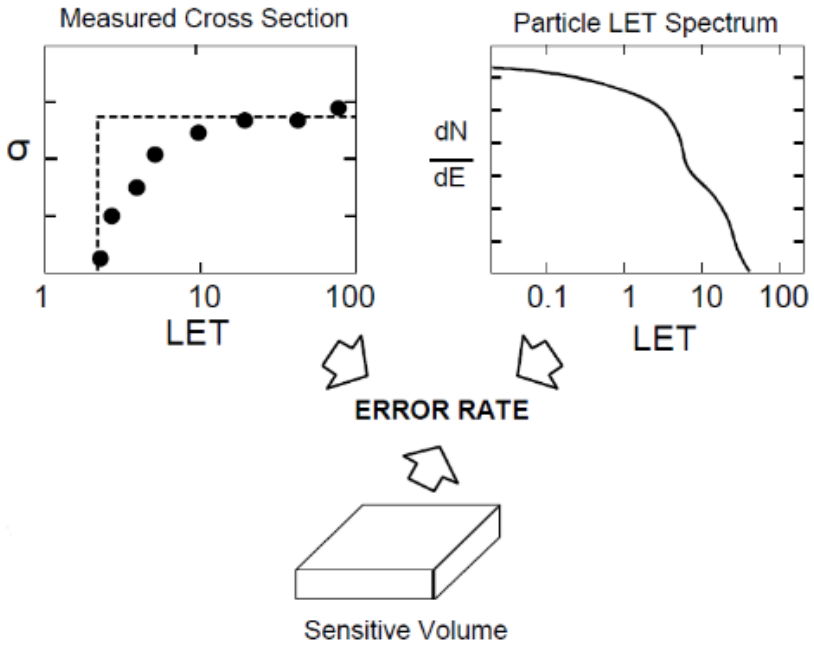

Figure 16: Rectangular parallelepiped SEU prediction consists of determining the SEU cross-section of the sensitive volume and combining the cross-section with the LET spectrum of a certain environment.

5.1.2 The effective flux approach

An alternative to the chord-length models for predicting heavy ion induced soft errors is the effective flux approach, introduced by Binder in ref. [55]. In the effective flux method the LET spectrum of the expected environment is converted into a spectrum of effective LETs incident on an SV with the shape of a thin lamina. The concept of effective LET is based on the assumption that by increasing the angle of incidence of the incoming ion the path length within the SV is increased by the cosine law. The effective LET means that instead of the path length the LET is considered to increase:

$$LET_{eff} = \frac{LET}{\cos(\phi)}.$$

The basic idea behind predicting the SEU rate is to first measure the SEU cross-section as a function of effective LET, obtain the flux of the radiation environment as a function of effective LET and combine these. This way, the effective flux approach is

independent of path-length distributions. For LET values above the threshold LET an upset will occur. For LETs below the threshold there exists an angle at which it produces an upset. A cut-off angle is needed in order to prevent very long paths. The effective flux method has been shown to be equivalent with the RPP model when the assumption of a thin SV is valid. As it is a LET-based prediction model with a single critical energy it has inherently the same faults as the RPP model.

5.2 Traditional proton SEU rate prediction

Protons' contribution to SEUs is accounted for their ability to cause nuclear reactions resulting in highly ionizing heavy ions. There have been methods to estimate proton induced SEUs since the 1980's both by nuclear reaction analysis methods and semi-empirical methods.

The semi-empirical approaches use a similar method as the IRPP method for heavy-ions. First, an experimental proton upset cross-section versus energy must be determined and described by a function, usually a log normal or Weibull function. After this, the expected proton spectrum of the orbit is taken, possibly converted to a spectrum inside a shielding, and combined with the upset cross-section to find the SEU rate. The difference to the IRPP method is that with protons the path-length distribution is not used.

The nuclear reaction analysis methods are based on the basic reaction processes and their cross-sections in materials. The secondary nuclei and their energies depend on the reaction and several papers have analyzed the energy depositions from these events either analytically or Monte Carlo simulation. Miroshin and Tverskoy derived an equation for the proton SEU rate due to inelastic nuclear collisions:

$$\sigma = n \cdot V \cdot \sigma_{in} \cdot \epsilon(E_{thr}),$$

where n is the number of atoms in a volume of certain material (silicon), V is the volume of the SV, σ_{in} is the cross-section for inelastic interactions with the material of the SV (Silicon) and $\epsilon(E_{thr})$ is the fraction of interactions which deposit energy exceeding the critical energy [56]. This method excludes energy depositions due to elastic collisions as well as the complexities associated with particles leaving the SV and contributions from nuclear reactions taking place outside the SV. The inherent complexity related to addressing these shortcomings indicates the need for a different approach, such as a Monte Carlo simulation method.

5.3 Present SEU rate prediction techniques and challenges

5.3.1 SEUs from nuclear reactions

While the (I)RPP rate prediction models have been successful in predicting the on-orbit SEU rates [45] [57], the simplicity doesn't come without its limitations. The

assumption that particles with same LET induce the same amount of errors has been shown to fail in regions where nuclear reactions dominate the response [58]. When an incident particle induces a nuclear reaction nearby or within the SV of a device much larger charges may be deposited into the SV as opposed to what could have been deposited based on the incident particle LET. Figure 17 illustrates how incorporating nuclear reactions in the charge deposition simulation creates an additional branch of high charge deposition events.

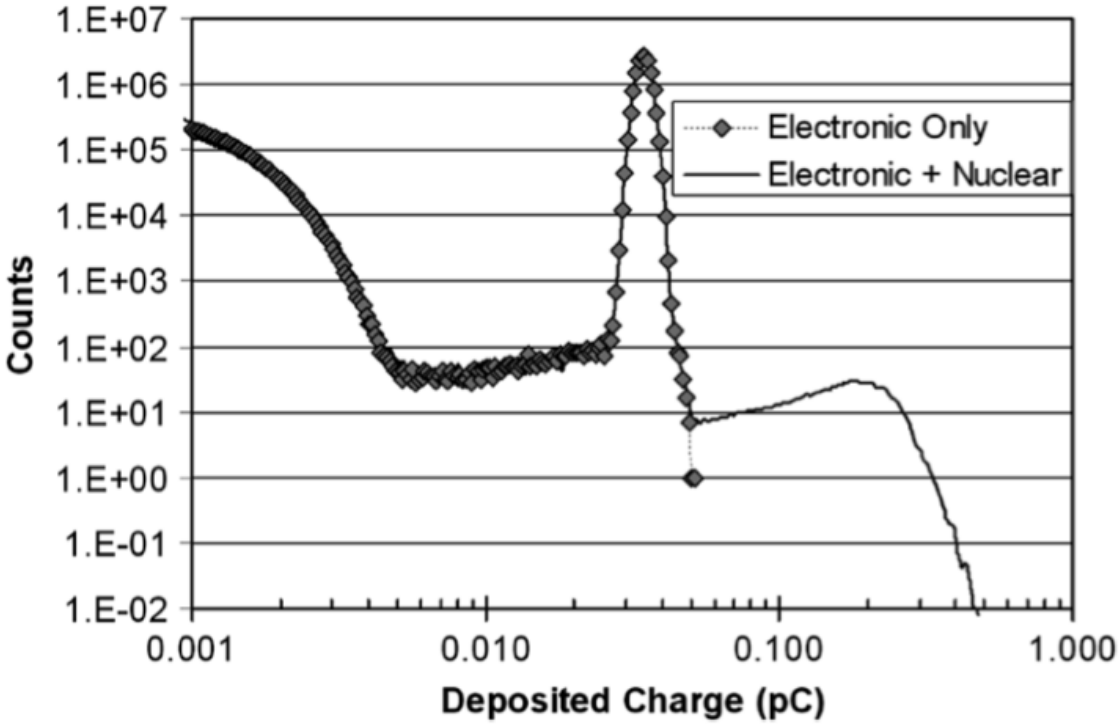

Figure 17: Including nuclear reactions in the charge deposition simulation shows the contribution of nuclear reactions to high deposition events. [58]

The knowledge of the particle type and energy is shown to be more important in these areas, as particles with LET smaller than the threshold LET are able to cause upsets. In ref. [59]–[60] it is shown that different particles sharing the same LET value could lead to differences of more than one order of magnitude in SEU cross-section. This is shown also in figure 18. One presented implication is that for devices which are not susceptible to SEUs due to the energy deposition from direct ionization of the primary particle, the SEU cross-section depends strongly on ion species and, for example, the nuclear reaction cross-section. Until recent years, the effects of heavy ion nuclear reactions in SEU rate predictions have mostly been neglected.

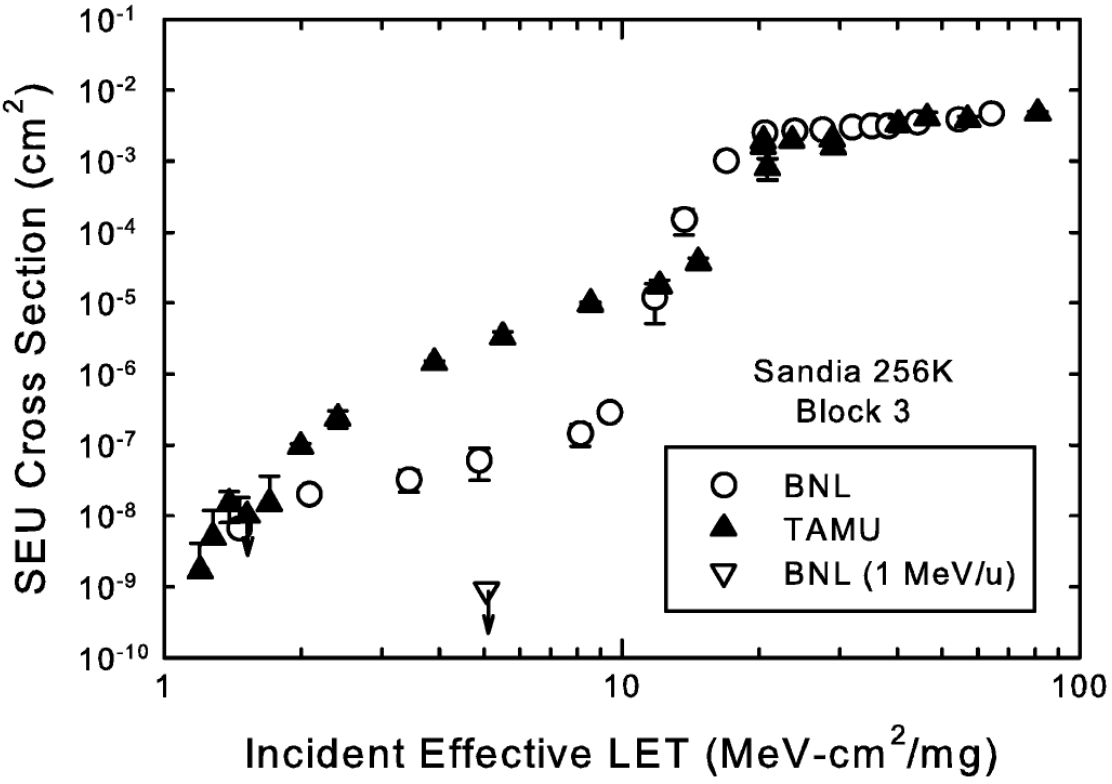

Figure 18: SEU vs. LET [60].

5.3.2 SEUs in modern technology

As technology scales to smaller dimensions new problems may be introduced. Figures 19a and 19b show the evolution of the atmospheric neutron induced SEU rates in DRAM and SRAM technologies. Figure 20 shows the observed SEU threshold charge as a function of feature size, surprisingly showing very little dependence on device technology.

In scaled CMOS devices, such as an SRAM memory, the decreasing amount of charge representing stored information has decreased the SEU threshold. In SRAM memories, the memory type commonly used in space applications, the SEU sensitivity was steadily increasing due to device scaling, until it started to decrease a few technology generations ago. The turn was explained to result from decreased charge collection efficiency in scaled sensitive volumes [61]. Nevertheless, predicting the soft error sensitivity of future technologies has proven to be difficult as completely new effects may start to occur.

As seen in figure 19a, the soft error hardness trend is very different for DRAMs than for SRAMs. The SEU hardness has actually increased in modern DRAM memories, the memory type used in, for instance, personal computers. Before, the concern

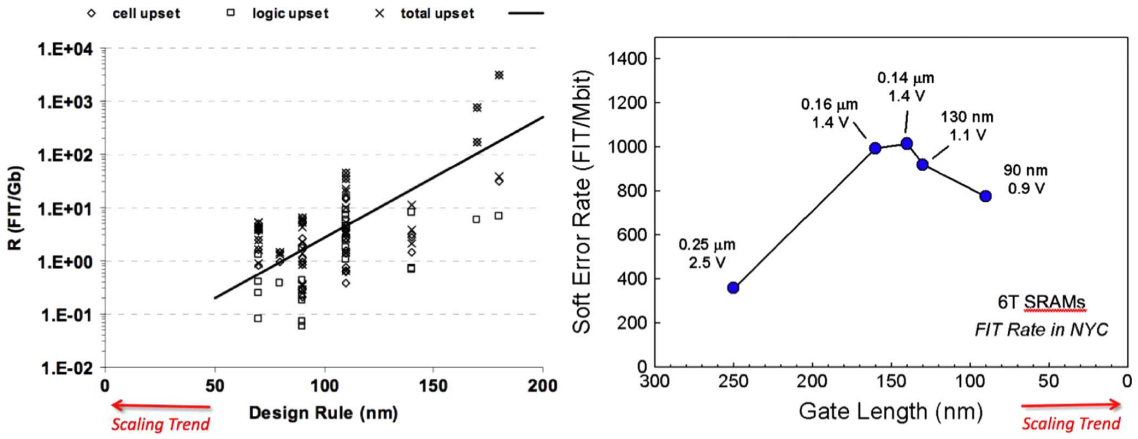

Figure 19: The soft error rate versus technology scaling in (a) DRAM and (b) SRAM. FIT = 1 error / 10^9 operating hours.

was that the trend of decreasing operating voltages would increase the soft error rate as particles with lower energy would be able to cause errors. However, the scaling of the DRAM cell size has been faster compared to that of the storage capacitance making it less probable for an incoming particle, such as an atmospheric neutron, to cause an upset [62], [61]. This indicates decreased SEU cross-section *per bit*. Nevertheless, it is important to realize that even though the soft error rate per bit has decreased, the overall soft errors have remained roughly constant due to the increasing amount of bits crammed on a chip.

Traditionally protons have been considered unable to cause SEUs by direct ionization because of the relatively low amount of generated e–h pairs per unit track length when compared to heavy ions. Now, however, SEUs from direct ionization of low-energy protons have been observed for 65 nm and 45 nm technologies [63] [64] which were not included in figure 19b. Muon induced upsets were analyzed in ref. [65] and although the muon contribution to the soft error rate was found small in present 65 nm and 45 nm technologies it was considered likely to become of greater significance in future technologies with lower critical charge values. This is important not only for spacecraft electronics but also for terrestrial electronics, since cosmic-ray secondary muons constantly reach sea level.

The spatial distribution of the carriers generated by the ion will become important [66] in smaller devices. If the radius of the ion track is large enough SEUs may occur even when the ion itself does not hit the sensitive area. The impact of energetic delta rays in the SEU rate of a 22 nm SRAM was analyzed in ref. [67]. Their predictions are that these memory cells with very low critical charges can be upset by delta-rays, and that SEUs may occur even at tens or hundreds of micrometers away from the

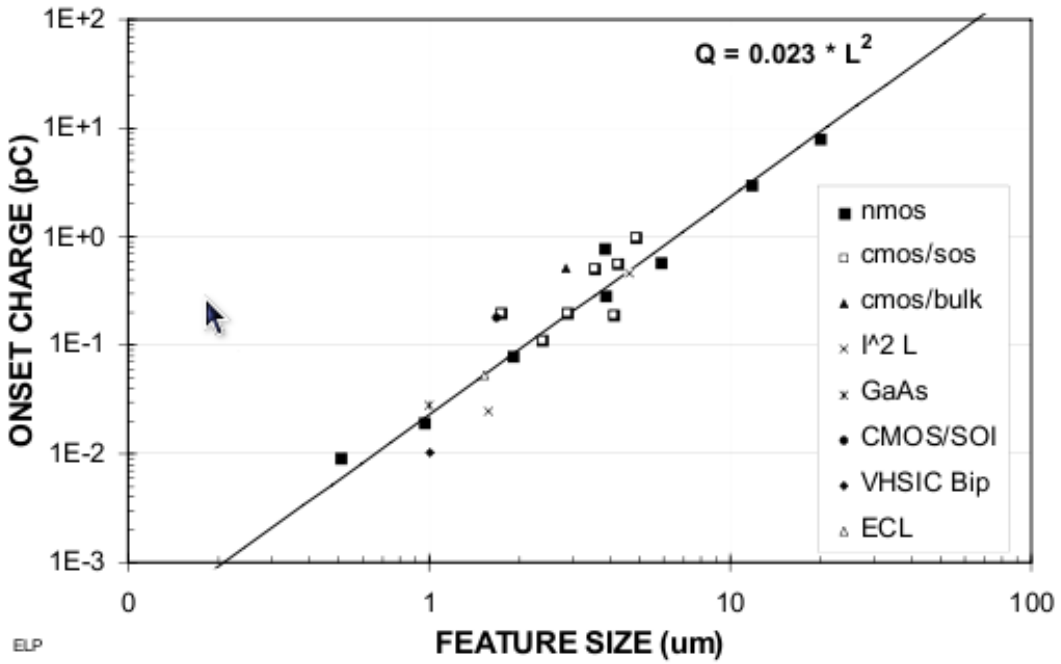

Figure 20: Observed SEU threshold charge as a function of feature size [45].

primary ion strike location. If the size of the ion track is comparable to the size of the SVs, multiple bit upsets may be induced [68]. The (I)RPP approaches cannot account for MBUs since the charge is assumed to be collected at a single transistor.

Modern electronics include several metallization and dielectric including heavy elements such as gold and tungsten above the circuitry. The presence of these layers containing heavy material in the vicinity of an SV can affect the SEU cross-section. In ref. [69] the authors show with the help of a Geant4-based physics-simulation tool an increase in high charge collection events attributed to the enhanced cross-section for proton-induced nuclear reactions.

5.3.3 Physics simulators

Physics-based simulators can be used to overcome or alleviate some of the problems arising from the limitations of the RPP model. Such a simulator taking care of generating a flux of particles and propagating them through a geometry in a realistic manner includes the energy depositions from all known processes and incoming particles.

Monte Carlo simulators, algorithms relying on repeated random sampling, have become widely used in the SEE community to take care of the particle transport. Monte Carlo physics-simulators methods are a natural approach for simulating the

varying particle flux in space and the randomness of the energy deposition in a medium, which is a major source of inaccuracy in the LET-based approaches described above [70]. This would also remove need for the separate analyzes when estimating heavy-ion and proton contribution. Realistic physics simulator would also incorporate the direct ionization from protons as well as indirect ionization from heavy ions, both of which are lacking in the traditional methods but which may become important. Geant4 is an example of a widely used Monte Carlo simulation tool for simulating the transport of particles through matter. Geant4 will be discussed in more detail in section 6.

One way to utilize a physics-based simulator in SEU rate prediction is to simply extend the RPP model by achieving a more realistic energy deposition spectrum by including more physics processes. The concepts of a SV and a critical charge are still present and the enhancements in results are obtained by including contributions from all important physics processes, for instance, nuclear reactions and delta-rays. With detailed geometry descriptions, the effects of device overlayers can also be analyzed. Figures 21 and 22 visualize the applicability of a physics simulator in SEU prediction. Figure 21 visualizes a nuclear reaction event including the tracks of all the particles after the event. Figure 22 visualizes the penetration of an ion into a block of silicon where several SVs reside. The paths of the primary ion track and several delta-electrons are visible.

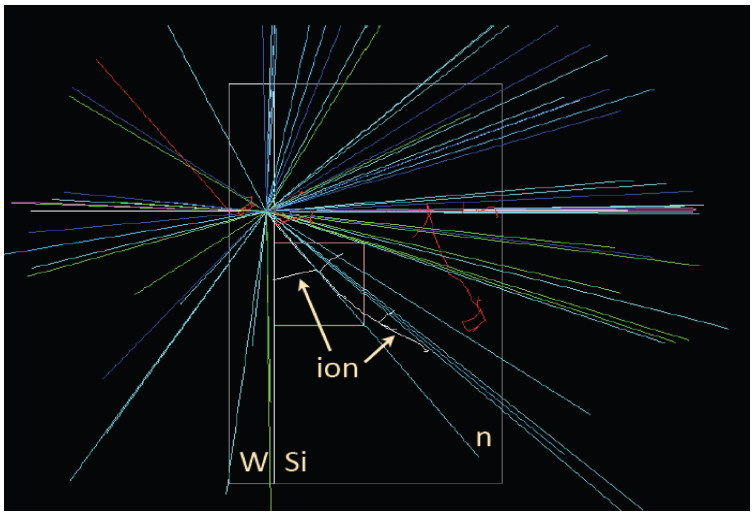

Figure 21: Visualization of a nuclear reaction in Geant4 simulation [71].

In ref. [72] the authors present measured on-orbit SEU data from the NASA's Messenger mission and compare the data to results obtained by using the traditional IRPP SEU rate prediction as well as by SEU prediction utilizing a particle transport simulator. The simulations were performed with a Geant4 program, MRED, and the

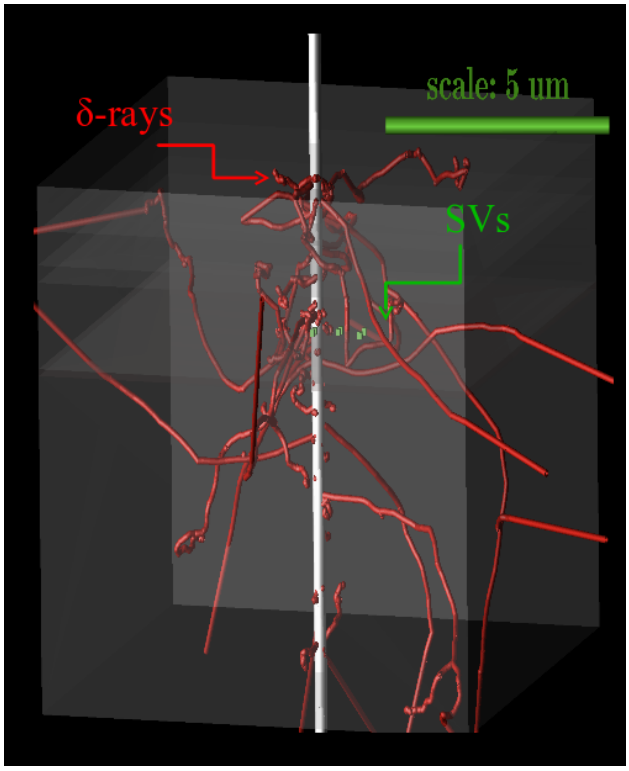

Figure 22: Visualization of a Geant4 simulation with an ion penetrating into a block of silicon [71]

geometries surrounding the SVs were described to be similar with the overlayers of an SRAM. The results of the comparison are shown in figure 23. Despite the large systematic error, the results obtained by using the physics-simulator are a great improvement over the traditional IRPP method. The results from MRED are in agreement with the observed data and the authors of the paper conclude this to be due to the more realistic physics, mainly indirect ionization events.

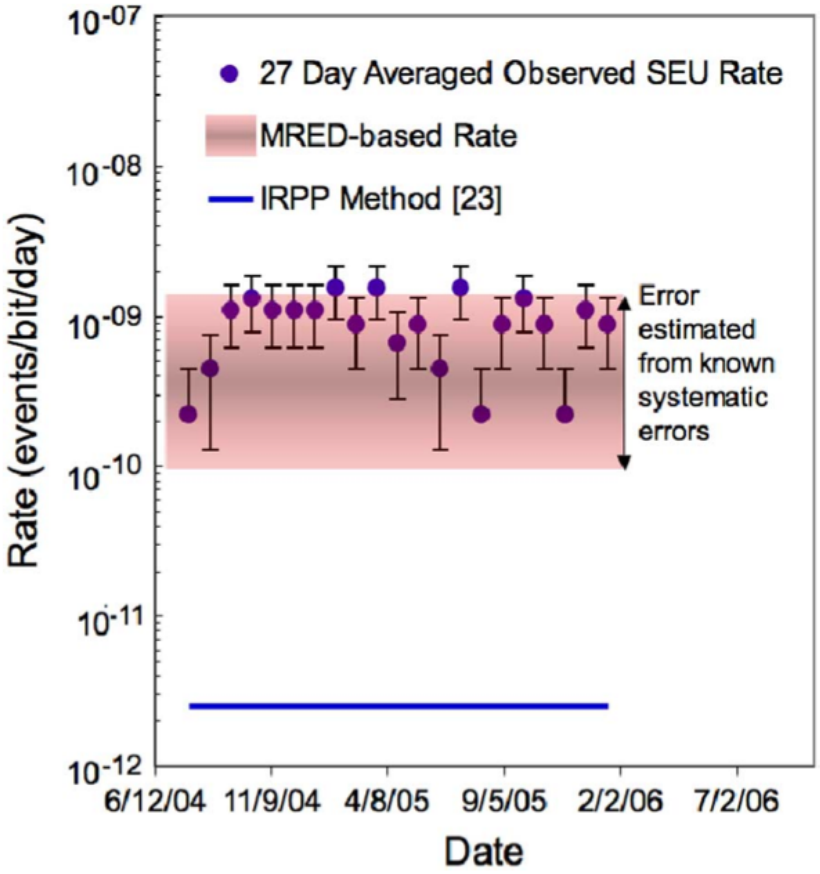

Figure 23: The predicted SEU rate obtained by using physics-based particle transport code (Geant4-based MRED) shows excellent agreement with the observed data [72].

A more advanced approach to SEU rate prediction utilizing a particle transport simulator is to combine it with other modern tools, such as a circuit modeling tool. A circuit modeling tool, for example SPICE, can determine whether a charge injection, obtained from the particle transport simulator, in a circuit will lead to an upset. This method is explained in ref. [73]. This method still includes the concept of a SV where the energy is deposited in the physics-simulator.

In refs. [74] and [70] a method of combining Geant4 and a technology computer aided design (TCAD) tool is presented. This enables the user to have a detailed device geometry within the Monte Carlo simulation for the energy deposition which is then coupled with the charge carrier transport solver of the TCAD tool. It is noted, however, that such a method needs an enormous amount of computation time making the simulation an exhausting task even for the current supercomputers in cases which involve realistic circuits consisting of several transistors.

6 Geant4

As an alternative to the traditional SEU rate prediction methods based on average energy deposition into a box-shaped SV, a method using Monte Carlo computation was mentioned above. For simulating the particle transport and energy deposition in a medium, a toolkit called Geant4 is a useful choice. Geant4 (GEometry ANd Tracking) is "a toolkit for simulating the passage of particles through matter" [75], [76] developed by the Geant4 collaboration. It is called a toolkit since it is not a program but a framework for creating simulation programs with the help of a well documented application programming interface and a large set of useful example programs. Geant4 is free, open-source, object-oriented and actively developed by a large number of individuals with expertise in programming as well as in physics. The design makes it possible for the user to extend or overwrite any part of the code with own implementations. Although Geant4 was first designed for simulating the detectors in high energy particle experiments, it is nowadays used also in nuclear physics as well as in space and medical technology.

6.1 An Overview of Geant4

Geant4 was designed with modularity and flexibility in mind, so that one can choose the needed components and that the modification of existing features and inclusion of new code is possible. Geant4 enables the creation of a desired geometries for the simulation, the event generation of energetic particles and ions, the tracking and hit management and, most importantly, provides for the physics for particle interactions in matter. Visualization of the geometry and particle tracks is also possible through different interfaces. Simulations can be controlled by the included user interface or run using macro files consisting of user commands. Each of these tasks provided by Geant4 are divided into separate C++ classes with well defined responsibilities and interfaces. This makes it possible for the massive amount of code lines to remain manageable, extensible and understandable.

The prerequisite for creating a functioning program with Geant4 is the knowledge of object-oriented programming, C++ language and physics related to the simulation. The simplest Geant4 program requires the definition of the primary particles, the simulated geometry and the physics for the particle interactions. The physics can be chosen from available physics lists or constructed by including the required processes for simulated particles. The particle source and geometry must be defined by hand, but the code from the example programs can be used as a pattern when creating the first programs.

Geant4 enables the user to control each part of the simulation by providing so called hooks. With the help of hooks the user can add desired operations which are performed during the run of the program. For example, the user hooks enable

the calculation and printing of energy depositions in a calorimeter by an ionizing particle. The user has to take care of saving any generated data since Geant4 does not automatically print or store anything from the simulation. A certain part in the simulation geometry can be defined as a sensitive detector, with the help of a Geant4 *G4SensitiveDetector* class, and when a particle traverses in this volume a user hook method is activated. This way the user can implement the desired features, e.g. create graphs and histograms already during simulation, save raw data, etc.

As a first step of using Geant4 in the SEU rate prediction, the most important part of the accuracy of the simulation is the physics. The open and object-oriented design makes it possible for the user to see how the physical processes, cross-sections and final states are computed. For example, cross-section computations using formulas can be replaced with user-written code and cross-sections from interpolation of databases can be switched to use user-defined databases. Same applies for the final state computation. The accuracy and validation of physic models is described more in the following sections.

Several complete simulation programs using Geant4 exist. Examples of such tools are MULASSIS for multi-layered shielding simulation and dose and particle fluence analysis [77] [78], SPENVIS (Space Environment Information Systems) [79] [80] and G4beamline for the design and evaluation of beam lines [81].

6.2 The Geant4 kernel and simulation flow

Geant4 kernel is responsible for managing the tracking of particles through the geometry and fields, managing the processes registered to particles and tracking optimization. *Tracking* in Geant4 is a hierarchical system consisting of events, tracks, steps and respective manager classes. Tracking manager class brokers transactions between *event*, *track* and *tracking* categories. Tracking does not handle particle transport as in Geant4 it is a process.

Events contain the primary particles and vertexes before the processing, the hits and digitizations after processing and optionally the trajectories of simulated particles. The simulation of particles movement advances in *steps* and the respective `G4Step` class includes the two endpoints of a step, pre-step point post-step point, containing the points' position and the volume where the particle exists. The change in track properties between the two points, such as a change in energy and momentum, is also stored in `G4Step`. *Tracks* carry information, for example, of current time-space position of the particle and a pointer to the physical volume where particle currently exists.

A run is the largest unit of simulation, and several `beamOn` method calls representing several runs can be given in one `main()` of the program. The `main()` method in a Geant4 simulation can be very simple. What is required is the instantiation of *G4RunManager*, initialization of the simulated geometry, the physics list, the primary

generator and the Geant4 kernel. Invoking the run manager's `beamOn` method starts a simulation *run* consisting of any given number of consequent events.

Before and between separate runs commands can be given to the Geant4 user interface manager to control the simulation. Commands can be given hard coded in the `main` method, in an external macro file or interactively via the Geant4 (graphic) user interface. This way the particle type and energy, verbose level or visualization settings, for instance, can be changed. User's hooks enable the user to include code which is run before, in between or after runs, events, tracking and steps.

6.3 Geometries in Geant4

Geant4 allows the creation of complex and realistic geometries. The concepts of *solid* and *logical* and *physical* volumes are essential in Geant4 geometry. Logical volume is defined to represent a detector element with a certain shape and with logical relations to other parts in the geometry. A logical volume can contain other volumes and it can be defined as a sensitive detector, as mentioned above. Attributes such as the material of the volume resides in the logical volume. The concept of solids give the shape and size to a volume whereas physical volumes define the positioning of the logical volumes in the enclosing volume.

In Geant4 it is possible to create elements from isotopes and materials from elements, and then assign these to logical volumes. The materials can be constructed from one or more elements or mixtures, and contain information about the density, temperature, pressure and state. Also electric and magnetic fields can be created.

The basic way of defining geometries in Geant4 is typing it in the code. Simple shapes, such as boxes, spheres and cylinders, can be created with the Constructive Solid Geometry. More complex shapes can be obtained by Boundary Representations where the solids are defined by their bounding surfaces. The bounding surfaces can be planes or higher order surfaces. Geometries can also be defined from CAD models since Geant4 solid modeler is compliant with STEP (Standard for the Exchange of Product model data), an ISO standard defining data exchange between CAx (such as CAD) systems [82]. It is good to use as simple shapes and geometries as possible, because complexity increases the computing time as well as the time spent on writing the code.

6.4 Cuts

In Geant4, all generated particles will be tracked until they stop or go outside the simulation world. So called production cuts are defined to set a threshold for particle generation. Production cuts are given in range, which is then converted to energy for all materials. Particles that would have a range below this threshold are not generated and the corresponding energy is deposited into the medium. This is done

to avoid the generation of massive amounts of low energy particles from, for example, bremsstrahlung. Since all generated particles are tracked to zero kinetic energy, production cuts don't affect particles' range in material. The values for production cuts affect the accuracy for the local energy deposition in the material and simulation computation time. Some processes, such as particle decay, can have their own production cuts, and if the distance to a geometrical boundary is smaller than the defined cut, the production cut can be omitted. Different cuts can also be applied for different particles and to different parts of the geometry.

6.5 Geant4 Physics

The selection of the physics used in a Geant4 simulation must be done carefully in order to obtain the best results. Each particle must be associated with the physics processes relevant to the simulated scenario. All required particles and processes are usually instantiated in so called *physics lists*. Instead of creating a physics list from the very beginning it is often useful to utilize and modify existing, predefined physics lists.

All physical processes in Geant4 conform to the interface of the base class *G4VProcess*. Physical processes are divided into several categories, such as electromagnetic processes, hadronic processes and particle decay. Transportation of the particles is also a similar process in Geant4 since particles are not self-moving but transported step by step by the transportation process. The step length is a significant factor to the execution performance and tracking precision. The step lengths are modulated by the associated physics processes and by the user. The actions of physics processes may take place along these steps, after a step or while the particles are at rest.

The Geant4 physics processes include two important methods, `GetPhysicalInteractionLength` (GPIL) and `DoIt`. The GPIL method returns the proposed step length from the current position to the next one. In the case of a particle decay, for example, this is calculated using the mean life of the particle. The process which returns the shortest interaction length is selected to take place in an unbiased manner. `DoIt` method then implements the interaction by generating the final state, i.e. changing the particle's energy, momentum and direction and the producing secondaries. A single process can be implemented with different *models*, which can alternative or complementary to each other. Certain model may be more applicable depending on the particle type, energy range and material.

The important physical processes for investigating SEE are electromagnetic processes, hadronic processes and transportation. Electromagnetic processes at energies higher than a few keV are rather well understood and modeled in Geant4. With hadronic reactions the distribution of secondaries is a problem, and for ion-ion-reactions the proposed minimum energies to be used with the existing models are higher than what are available in many accelerator laboratories.

6.5.1 Electromagnetic physics models

Geant4 covers a wide range of electromagnetic interaction processes including, but not limited to, ionization, Bremsstrahlung, pair production, Compton scattering and photoelectric effect. The *standard* electromagnetic process category contains classes for handling the energy loss of electrons and processes due to ionization and the related to scattering processes as well as delta-ray production. The energy loss due to soft as well as the discrete simulation of hard bremsstrahlung is also included. For hadrons, the ionization energy loss and delta-ray production is included. The standard category also includes the simulation of ionization, bremsstrahlung and delta-ray production for muons. In each case, the energy losses also depend on the production cuts described in 6.4.

The energy range of the standard electromagnetic model in Geant4 extends from 1 keV to 10 PeV [83]. With the *low energy* extensions energies down to 100 eV and even below can be reached [84].

A model for screened Coulomb scattering between nuclei was developed outside the Geant4 collaboration for describing the energy deposition in the form of atomic motion (recoil nuclei from elastic collisions) [85]. Similar model developed by the Geant4 collaboration also exists, but the screening of the atomic electric field is not taken into account and the computation speed is much slower.

The electromagnetic models of Geant4 were compared against data of the National Institute of Standards and Technologies (NIST) and the International Commission on Radiation Units and Measurements ICRU in ref. [86]. This papers shows that several different parameters simulated with Geant4, such as mass attenuation, Compton interaction, photoelectric and pair production coefficients, are in good agreement with the reference data. The good agreement with data is also shown and explained [83] and references therein. The transport of ions in medical applications is presented in ref. [87], showing good results in predicting the ranges and depth-dose curves of the simulated ions.

For SEU rate prediction ionization is the most important interaction process to be simulated accurately. In addition to the ionization of the primary particles, also the secondary ionizing particles must be taken into account. This requires the ability to simulate the processes creating the secondaries, for instance nuclear reactions.

6.5.2 Nuclear physics models

Geant4 includes several theory driven and parametrized nuclear physics models for different energy regimes. At high incident particle energies, roughly from few GeV/u to ~TeV/u, three quark-level models exist, the quark-gluon string model (QGS or QGSP), the Chiral Invariant Phase Space Decay (CHIPS or QGSC) [88] and the Fritiof model [89]. These models are applicable to protons, neutrons, pions and kaons but cannot be used with ion projectiles. No model at these energies exists in Geant4 for

describing the nuclear interactions of ion projectiles.

At medium energies, from 50 MeV/u to roughly 10 GeV/u, the quantum mechanics based quantum molecular dynamics (QMD) model and two cascade models, the binary cascade and the Bertini cascade model, exist. Of these, the QMD model and the extension to the binary cascade model, the binary light ion reaction model, can be used for ions, whereas the Bertini cascade is not applicable to ions.

In the QMD model the interactions of particles are derived from the laws of quantum physics. The QMD model in Geant4 is adapted from the Jaeri QMD (JQMD) code [90] in which the reaction progresses in two steps: first, the direct reactions, non-equilibrium reactions and dynamical formation of fragments are computed, then the evaporation and fission decays are performed for the excited particles produced in the first step [91].

All the target and projectile nucleons are considered as participant particles in the QMD model. Each nucleon state is represented by a Gaussian wave function, and the total wave function of the system is assumed as the direct product of these. The time evolution is described by Newtonian equations and a stochastic two-body collision term [92]. The details of the QMD code in Geant4 are explained in ref. [93]. Figure 24 shows a schematically how a nuclear reaction progresses in the QMD model.

The binary cascade model in Geant4 is an intra-nuclear cascade model for the simulation of interactions of protons, neutrons and pions with nuclei [94]. An extension of the binary cascade, the binary light ion reaction model, exists for the simulation of ions as primaries. In the binary cascade model, the nucleus is described as a 3-dimensional collection of hadrons, and the projectiles interact with the target in binary collisions, i.e. between the primary particle and an individual nucleon of the nucleus. In the binary collision approach the paths of particles are simplified to be straight lines before and after collisions. Geant4's binary cascade model can be seen as a hybrid between a classical binary cascade code and the QMD code due to the binary collision approach and the 3-dimensional model of the nucleus derived from the direct product of the Gaussian wave packets of each nucleon.

The binary cascade model generates the secondaries and propagates them throughout the nucleus until they are absorbed, re-scattered or ejected. The secondaries may also undergo collisions and create a cascade. When the mean energy of all the particles in the system is below the cut-off value the cascade stops and the treatment of the system is delegated to a pre-equilibrium decay code. The transport sequence of the binary cascade is shown schematically in figure 25. According to the Geant4 physics reference manual [84], the binary cascade code transports light ions with, mass number less than 13 or with mass number below that of the target. This works more as a guideline and the model can be used with any ions, but with questionable results.

Experimental cross-sections are used directly or as a basis for parametrization. The cascade starts with a primary particle and the description of the target nucleus and stops when the mean energy of the particles in the system is below the cut-off

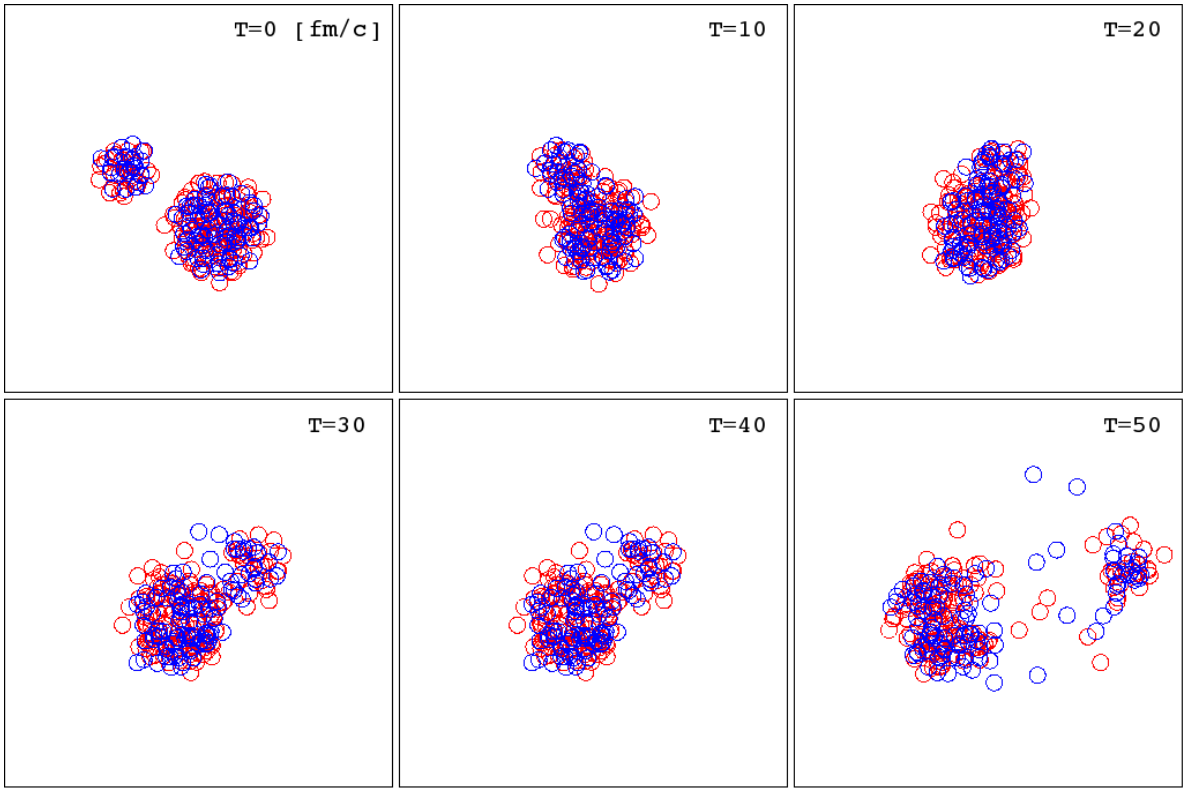

Figure 24: The time evolution of the reaction of 290 MeV/n Fe colliding with Pb, computed with QMD [93].

energy. After this, the evaluation of the system is passed to a pre-equilibrium decay code, described below. The mathematical details of the models are explained in ref. [94].

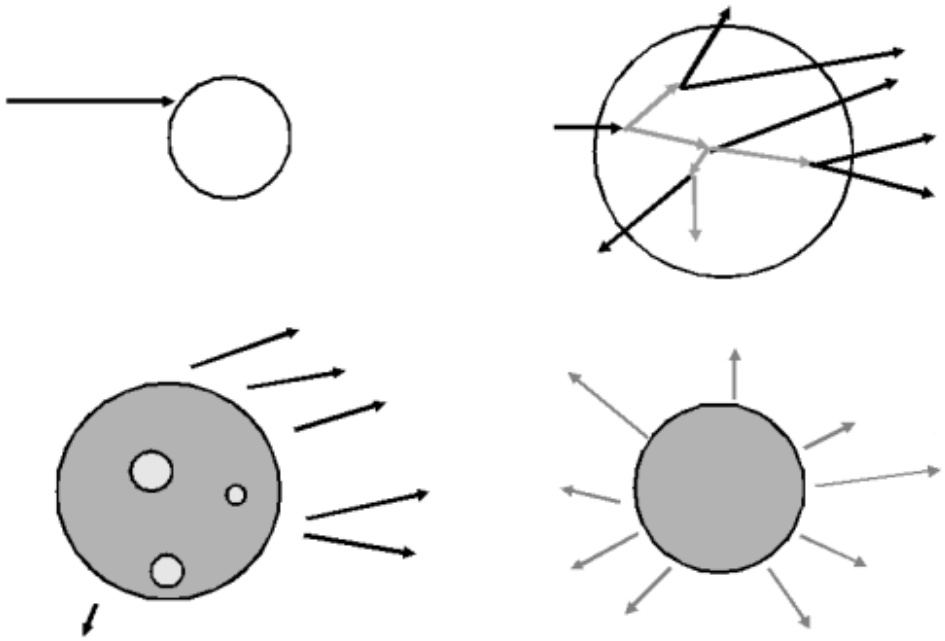

Figure 25: A schematic picture of the modeling sequence [95]. The primary particle creates a cascade inside the nucleus after which some high energy particles depart the nucleus. Lastly, the excited nucleus de-excites and undergoes evaporation.

Three major differences exist between the QMD model and the binary cascade model in Geant4. The particle tracks in binary cascade are handled sequentially, whereas QMD tracks particles simultaneously. Secondly, while in binary cascade reactions only take place between a primary particle (or a secondary) and the target, in QMD participant–participant reactions are naturally included as there exists no criterion between a participant particles and others.

Lastly, the quantum mechanical operator corresponding to the total energy of the system, the Hamiltonian, used in the equations of motion is calculated in the binary cascade model using a time-independent nuclear potential known as the optical model. The optical model is a macroscopic approach to construct a single potential for the whole nucleus. In the QMD model the nuclear potential is computed considering all the nucleon components in the system.

These differences result in QMD offering a more accurate and detailed, but also time-consuming, simulation compared to the binary cascade. The lack of a way for

treating participant–participant reactions is seen as a reason why binary cascade is not recommended to be used for simulating heavy ion reactions [93].

At energies below 50 MeV/u, Geant4's pre-equilibrium (precompound) model is used to bring the system to the equilibrium state. In the pre-equilibrium state, fragmentation into nucleons or ions under the influence of Coulomb repulsion may occur. A reaction can be passed on to the precompound model when the system has reached certain energy after being evaluated by the binary cascade or QMD model, and if the energy of the incident particle is below a certain threshold the nuclear physics is computed solely by the precompound model.

The final stage of a nuclear reaction is determined in the equilibrium de-excitation phase, where the nucleus is brought to the ground, low-lying excited or disintegrated states [96]. Several different low-energy de-excitation mechanisms compete in this phase, including evaporation, fission, Fermi breakup, multifragmentation and photon evaporation. This phase is also important to the formation of fragments and partitioning of the remaining momentum. A good reference for all these models used in different energy and simulation phases is the Geant4 Physics Reference Manual [84].

The limited amount of available experimental data on short-range heavy fragments from nuclear reactions, according to [97], complicates the validation of the simulation models. Validation of the models described above with experiments have been made by comparing the secondary neutron production in different reactions. In ref. [98] it is shown that both models, the binary cascade and the QMD, simulate the production of secondary neutrons fairly well with some disagreement. However, the ability to create fragments, e.g. from spallation and fission reactions, which are essential for accurate SEU rate prediction, is not demonstrated.

In ref. [99] the production of ^{16}O fragments from 180 MeV proton beam incident on an Al target using the binary cascade is compared with the experimental results obtained in ref. [100]. This comparison, also shown in figure 26 shows a significant discrepancy between the simulation results and the experiment. Similar comparisons using the QMD model within its valid energy range were difficult to find. In figure 27 is shown the comparison of isotope production between the QMD and the binary cascade model. In this case, the QMD model performs fairly well compared to the binary cascade model.

In ref. [101], the author produces a rather disappointing figure by simulating the ^{8}Li production from ^{7}Li (d,p) ^{8}Li reaction. This is shown in figure 28. It must be noted, however, that the measured results were gathered at energies which are mostly below the valid energy regime of the used simulation models. In the same study, the author also examined the production angles and compared them to the theoretical predictions. The theoretical predictions were obtained by setting the velocity of the target particles to zero and not considering the intra-nuclear momentum exchange. The expected theoretical behavior is shown in figure 29 and the simulated results are shown in figure 30.

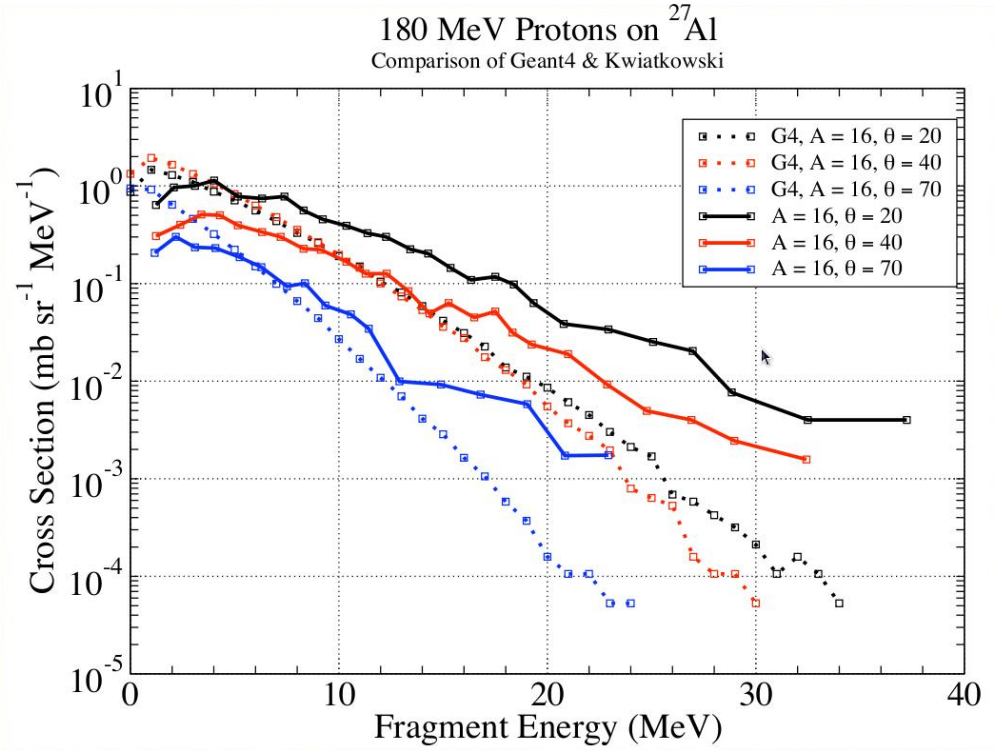

Figure 26: Comparison of the ^{16}O production from 180 MeV protons on an Al target [99].

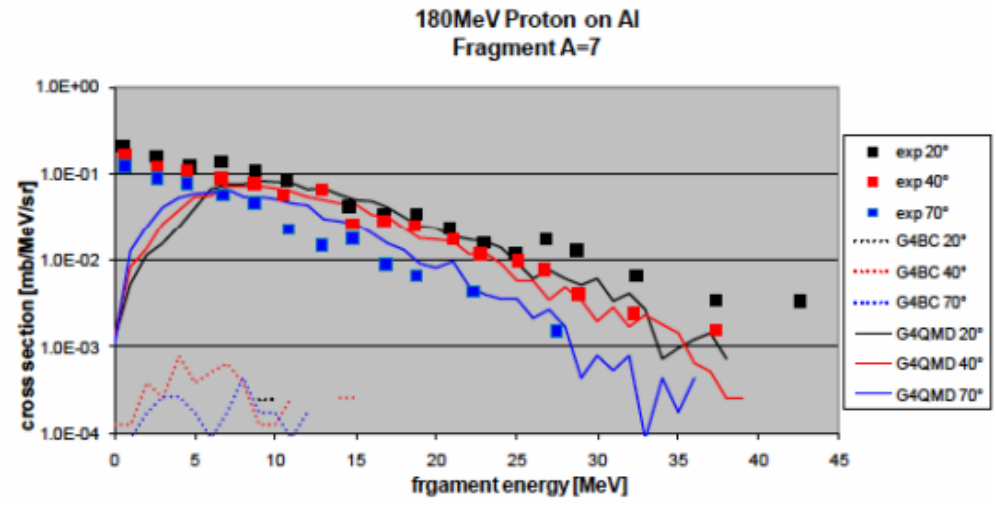

Figure 27: Comparison of isotope production between the QMD and the binary cascade using 180 MeV on Al and counting the fragments with mass number of 7 [98].

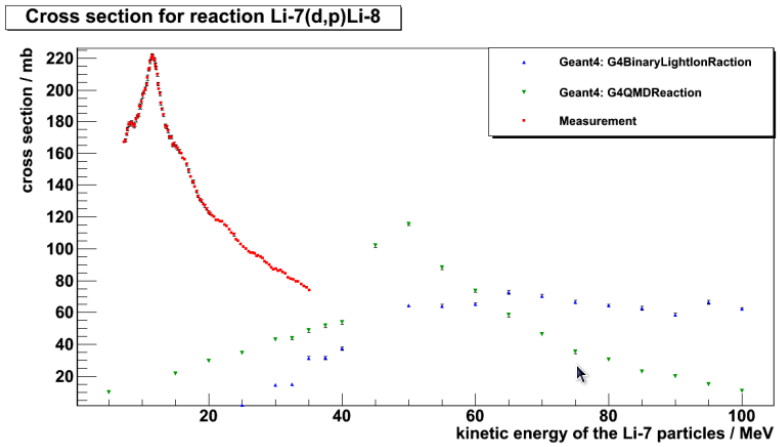

Figure 28: Geant4 simulation of ^{8}Li production using QMD and binary casacde models [101].

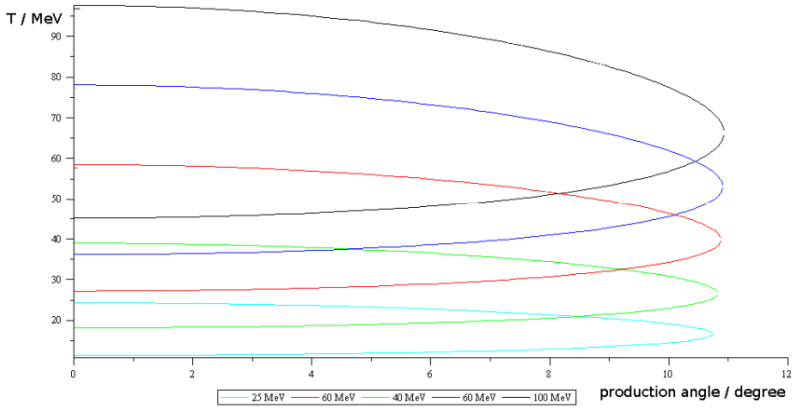

Figure 29: Theoretical expectations of the production angles of ^{8}Li in ^{7}Li (d,p) ^{8}Li reaction derived from kinematics [101].

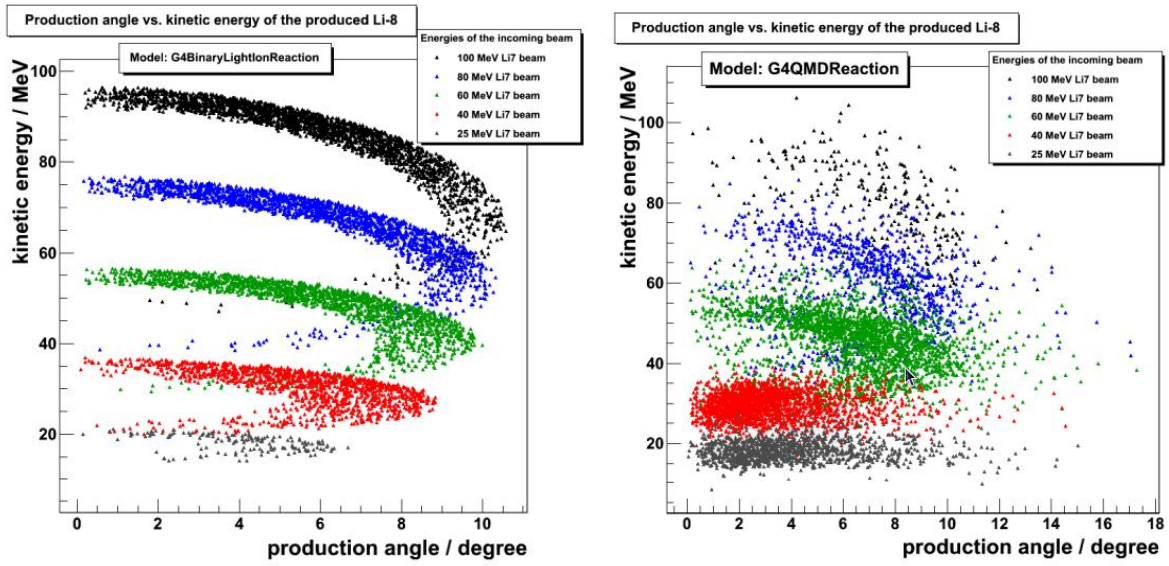

(a) **(b)**

Figure 30: Geant4 simulations of the production angles of ^{8}Li in ^{7}Li (d,p) ^{8}Li reaction by using the (a) binary cascade model, (b) QMD model [101].

The shape of the Bragg curve and the position of the Bragg peak, explained earlier in section 2.1, is primarily determined by electromagnetic interactions and straggling effects. Nevertheless, nuclear interactions (not to be confused with nuclear stopping) also affect the Bragg curve. Fragments from nuclear reactions may travel and deposit energy into depths which considerably exceed the position of the Bragg peak. This is shown in figure 31 as a tail on the right hand side of the Bragg peak, simulated with Geant4 using by the QMD and binary cascade models, together with the Geant4 electromagnetic models. The simulations were made by Lechner *et. al* [102] and show that these Geant4 models are capable of predicting the Bragg curve with good accuracy even in the tail region induced by nuclear reactions. In that study, the production of fragments was not studied in more detail.

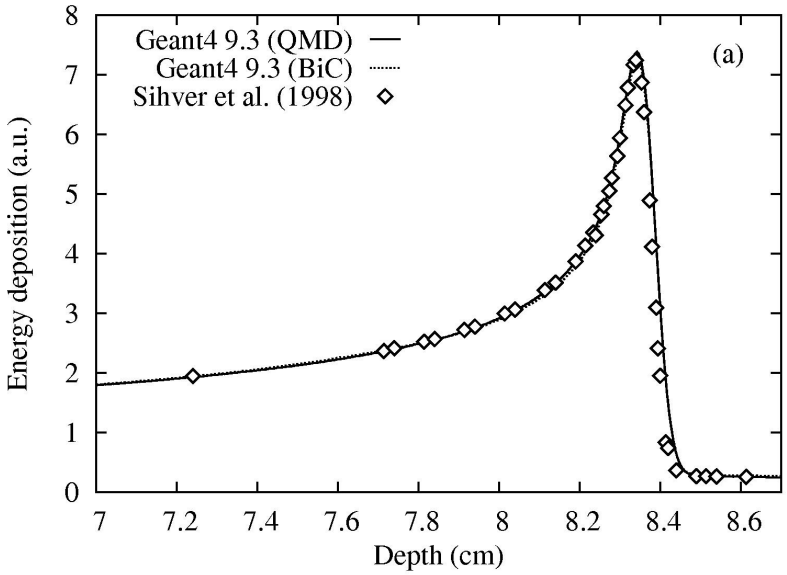

Figure 31: Simulation of the energy loss of 195 MeV/u ^{12}C ions in water [102].

7 Time-of-flight measurements and simulations

To gain more knowledge on the fragment production emerging from nuclear reactions, a time-of-flight (TOF) measurement was conducted in the RADiation Effects Facility (RADEF) in the University of Jyväskylä. The setup of the measurement is shown in figure 32. The beam comes in from the left and is first collimated and then directed onto the target. After the target, the outgoing particles are collimated and measured with a system which can be set up to a desired angle.

The TOF measurement is used as a technique for mass spectrometry. In the experiment, the primary ion beam produced in the JYFL K-130 cyclotron was guided onto a target consisting of heavy material such as gold or tungsten. The TOFs and kinetic energies of the outgoing particles were then measured and used to identify the particles. The flight time was measured between a multichannel plate (MCP) detector and a PIN diode, and the kinetic energy can be derived from the energy deposited into the PIN diode by the outgoing particle. The masses of the outgoing particles can be derived in the following way:

$$\begin{aligned} E_k = \frac{1}{2}mv^2 = \frac{1}{2}m\left(\frac{d}{t}\right)^2 \\ \Leftrightarrow \; m = 2E_k\left(\frac{t}{d}\right)^2, \end{aligned} \tag{8}$$

where E_k, m and v are the kinetic energy, mass and the velocity of the particle, d is the TOF base length and t is the TOF. The resolution of the masses depends on the resolution of the measured TOFs and on the energy resolution of the PIN diode responsible for measuring the E_k of the particles. Due to technical difficulties with the experimental setup, the E_k could not be resolved accurately and only the PIN channel numbers are shown.

The measurements were performed with three different target materials, gold, tungsten and copper, and with 9.3 MeV/A beams of ^{15}N, ^{56}Fe and 20 MeV/A beam of ^{15}N.

Similar measurements, although with a simplified geometry, were simulated by using Geant4. In the real experiments, the number of primary particles accelerated onto the target is of the order of 10^{12}–10^{13}. To match the number of primary particles of the real experiment in the simulations, one either needs a great deal of computing power or to come up with other solutions. These simulations were to be run on a single desktop computer, so a biasing techniques were used. The efficiency of the simulated detector was enhanced by enlarging the detector. The small detector area in a certain scattering and azimuthal angle was enlarged to a hemisphere counting events from all azimuthal angles for scattering angles between 0–90 degrees. The information of events in a certain scattering angle can be extracted from the data when

the location of the events on the detector is saved. In the simulation, two hemispherical detectors were used in order to get the time-of-flight between the detectors. The Geant4 simulation geometry is shown in figure 33.

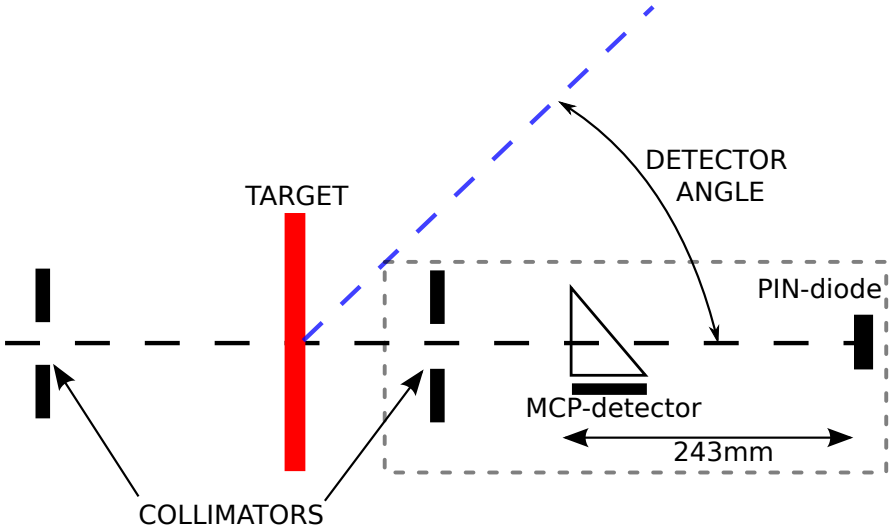

Figure 32: The time-of-flight measurement setup used in RADEF (not in scale).

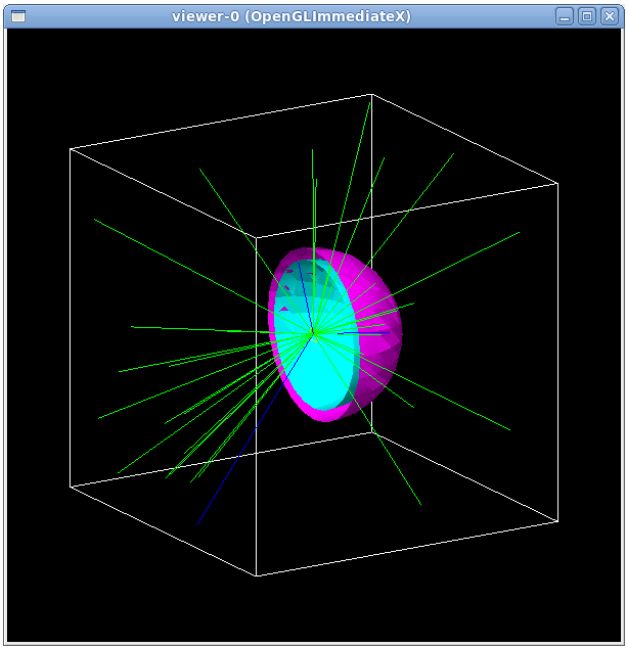

Figure 33: The used Geant4 simulation geometry.

As the probabilities for nuclear reactions are relatively low and most of the primary particles would simply go through the target without interacting strongly, the total reaction cross-section was enhanced by a certain factor. This factor is also considered a virtual enhancement for the number of simulated primary particles. One has to be careful when enhancing the total reaction cross section. If the cross-section is multiplied too much the incoming beam can be totally depleted in the first layers of the medium. The simulations in this work were performed with a cross-section multiplier of 10^4 and as the cross-section was only enhanced in the thin target foil, no depletion took place. Similar enhancing factor was also applied to the elastically Coulomb scattered particles.

The simulation runs consisted of 10^8 primary ions and the radii of the hemispheres in the geometry were 7.5 and 8.5 cm, which gives the TOF length of 1 cm. The selection of the sizes in the simulation geometry is rather arbitrary as their effect is canceled out when calculating the cross-section per solid angle. A comparison between the measured TOF curve and the one obtained from a Geant4 simulation is shown in figure 34. The total kinetic energy is shown on the y-axis and energy per nucleon on the x-axis. Due to the poor energy resolution in the PIN diode the y-axis in the figure can be used only qualitatively. With a lighter and a heavier particle having the same total kinetic energy, the heavier particle – being the slower one – will be drawn more on the left side of the figure and the lighter particle more to the right. The measurements and simulations show similar characteristics, i.e. heavy particles some recoil beam as well as lighter particles.

Two distinct separated regions of heavy particles, marked with green in the figure, can be recognized in the simulated scenario. The left part of the green region centers around 0.1 MeV/amu whereas the right part locates close to 1 MeV/amu. The left part, absent in the experimental figure, in simulation the part on the left part consists of elements with the mass around 200 u and the part on the right consists of elements with mass around 100 u.

The comparisons of the amount of produced fragments between the experiment and the simulations are made by discarding the left part of heavy (green) region from the simulations. From the results of the comparisons, shown in figure 35, it is evident that the simulation underestimates the production by more than one order of magnitude.

An interesting feature of the simulations is that changing the target material from gold to tungsten reduces the cross-section for particle production between masses 60–150 AMU by an order of magnitude. This difference occurs because in the case of tungsten target the simulation produces more target-like fragments and less fragments in the 60–150 AMU region. In the experiments, these two targets resulted in similar cross-sections. Also, it can be seen from figure 35 (top left vs. bottom left) that increasing the beam energy from 139 MeV to 300 MeV does not remarkably change the discrepancy between the simulation and the experiment.

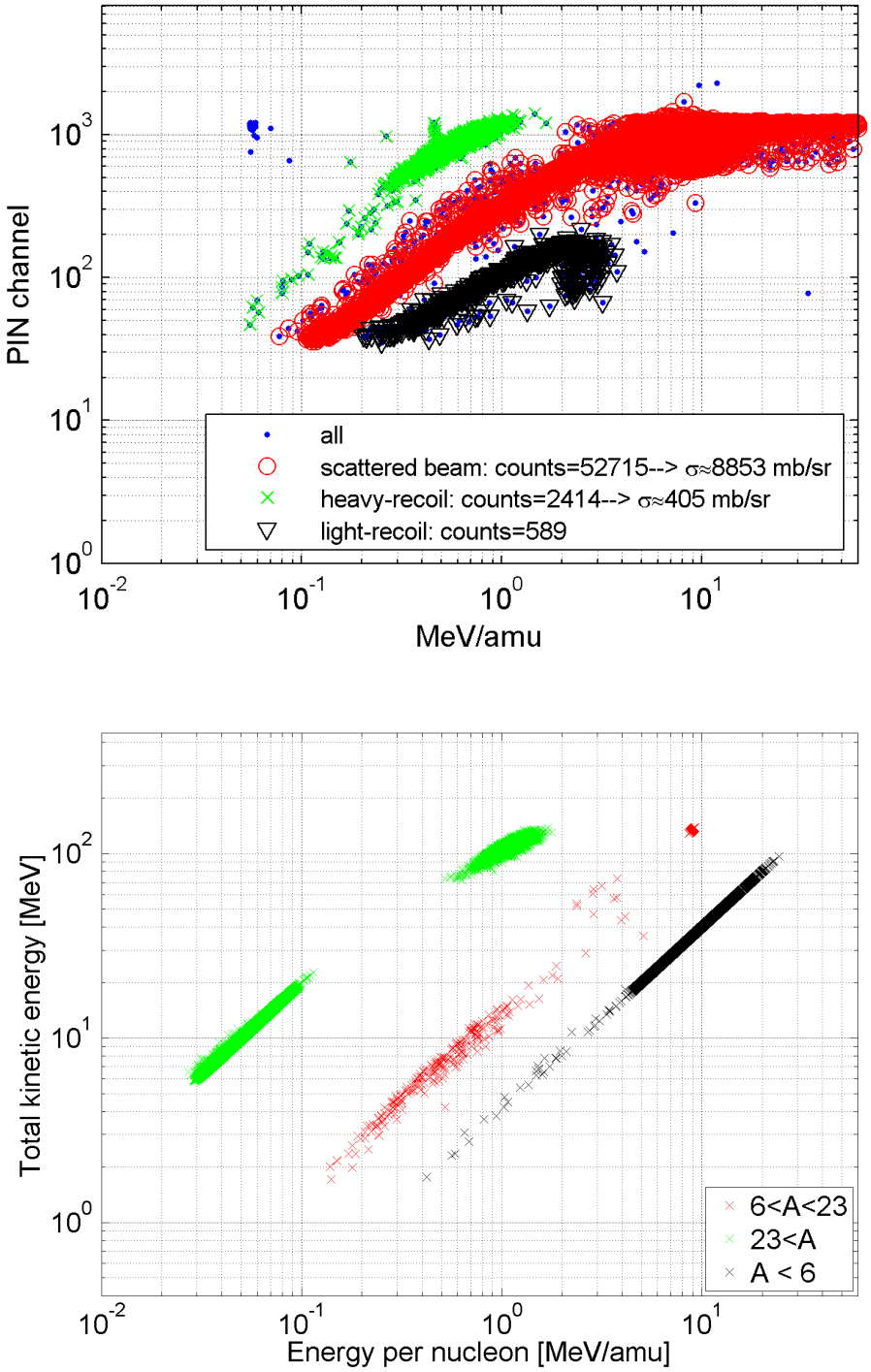

Figure 34: Energy (PIN channel) vs. time-of-flight (MeV/amu) from the experiment in RADEF (top) and energy (MeV) vs. time-of-flight (MeV/amu) from the G4 simulation (bottom).

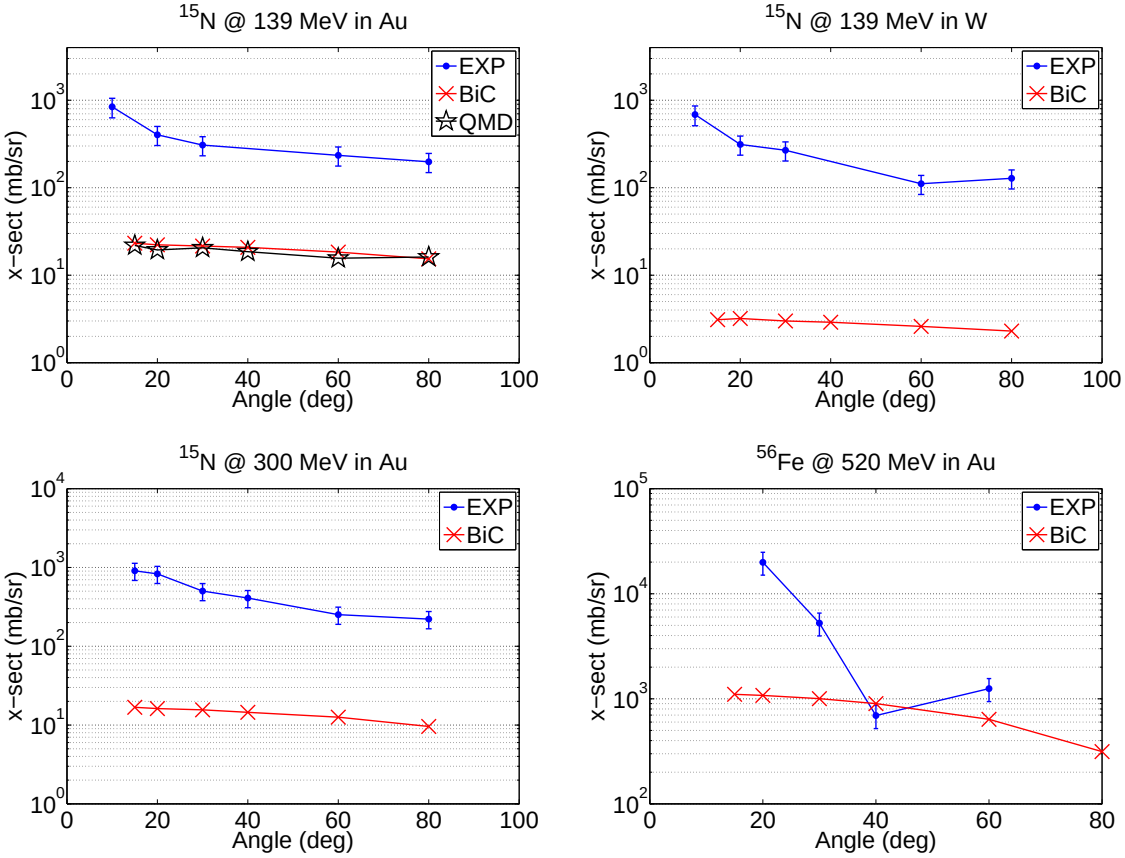

Figure 35: Experimental (blue solid dots) and simulated (crosses and stars) differential cross-sections as a function of scattering angle (in lab coordinates) for heavy fragment ($Z>Z_{projectile}$, cf. figure 34) production from different projectile (N and Fe) and target (Au and W) combinations at different energies. 139 MeV N^{15} in Au (top left) and W (top right), 300 MeV N^{15} in Au (bottom left) and 523 MeV Fe^{56} in Au (bottom right).

8 Conclusion

Radiation induces damage on electronics in space both on a short and long time scale. Single-event effects are produced by the energy deposition of a single particle and occur within the time scale of picoseconds. In this work, the basic physics and mechanisms behind one type of single-event effect, the single-event upset, and the methods used in SEU rate prediction are discussed.

Traditionally, nuclear reactions from heavy ions have mostly been excluded in the SEU rate prediction models. For modern electronics, the assessment of the energy depositions from nuclear reactions is required in order to predict the SEU rate accurately. However, the complexity related to estimation of the SEUs induced by the highly ionizing remnants of nuclear reactions renders the traditional, analytical SEU prediction methods impractical. Utilizing modern particle transport simulators in SEU rate prediction are one way to overcome this problem.

Many physics processes, such as nuclear reactions, are stochastic by nature and for this reason a Monte Carlo method, a method relying on repeated random sampling, is a practical approach for a particle transport simulator. Such a simulator, containing descriptions for all the relevant physics processes takes care of transporting the incoming particles through a given simulation world. Obviously, the accuracy of a SEU rate prediction method incorporating a particle transport simulator relies heavily on the validity of the physics models in such a simulator. For instance, no single theory explains the nature of nuclei and their interactions completely and progress in understanding the complex problem is made by using approximate models with limited range of applicability [17]. These models are usually limited to a certain energy range and particle type.

One particle transport simulator, the Geant4, is explored in this work. The validity of the nuclear reaction models used in Geant4 is put to test and compared with the time-of-flight measurements performed in the Radiation effects facility (RADEF) at the University of Jyväskylä. From the beginning it was predicted that, due to the difficulty of predicting the final states of nuclear reactions, the available computer codes would show significant disagreement from the experimental results.

Compared to the experimental results, the simulations are found to show more than an order of magnitude underestimation in the production of heavy fragments, which are the most essential constituents in the SEU prediction because of their high LET. Despite the strong underestimation in the fragment production, the produced TOF curves do exhibit similar features as in the measurements. Thus, even if the heavy ion nuclear reaction models are far from complete, they can be used to simulate similar high charge deposition events from low LET particles leading to SEUs which are observed irradiation tests. In order to improve the results, further research is needed to increase the understanding of the underlying physics and the quality of nuclear physics models.

By utilizing modern particle transport simulators, the possible susceptibility to new particles, such as delta-electrons and muons, and their contribution to SEUs can be studied. Particle transport simulator Geant4 does not handle the charge carrier transport due to drift or diffusion, which determines the endpoints of the created charge. Combined with other tools taking care of the charge collection and propagation in circuit, even more accurate results can be obtained. This method is also a step closer to developing a method from first principles, i.e. without any parametrization or empirical information.

References

[1] J.T. Wallmark and S.M. Marcus: *Minimum size and maximum packing density of nonredundant semiconductor devices*. Proceedings of the IRE, 50(3):286 –298, 1962, ISSN 0096-8390.

[2] D. M. Harland and R. D. Lorenz: *Space Systems Failures: Disasters and Rescues of Satellites, Rockets and Space Probes*, pages 24–25.

[3] D. Binder, E. C. Smith, and A. B. Holman: *Satellite anomalies from galactic cosmic rays*. IEEE Trans. Nucl. Sci, 22:2675–2680, 1975.

[4] G. E. Moore: *Cramming More Components onto Integrated Circuits*. Electronics, (8):114–117, April.

[5] C.A. Mack: *Fifty years of moore's law*. Semiconductor Manufacturing, IEEE Transactions on, 24(2):202 –207, may 2011, ISSN 0894-6507.

[6] J. F. Ziegler and W. A. Lanford: *Effect of cosmic rays on computer memories.* Science, 206(4420):776–788, 1979.

[7] E. Normand: *Single event upset at ground level*. Nuclear Science, IEEE Transactions on, 43(6):2742–2750, 1996.

[8] J. F. Ziegler, H. W. Curtis, H. P. Muhlfeld, C. J. Montrose, and B. Chin: *IBM experiments in soft fails in computer electronics (1978–1994)*. IBM J. Res. Dev., (1):3–18, ISSN 0018-8646.

[9] Jerrold T. Bushberg, J. Anthony Seibert, Edwin M. Leidholdt, and John M. Boone: *The Essential Physics of Medical Imaging (2nd Edition)*. Lippincott Williams & Wilkins, 2.00 edition, December, ISBN 0683301187.

[10] R. A. Reed: *Fundamental mechanisms for single particle-induced soft errors*. Nuclear and Space Radiation Effects Conference, Short Course Notebook, Section I, 2008.

[11] G. Berger: *Experimental tools to simulate radiation environments / radiation effects, part i*. RADECS Short Course, 2009.

[12] P. Sigmund: *Stopping power: Wrong terminology*. ICRU News, 2000.

[13] K. Krane: *Introductory Nuclear Physics*. "John Wiley and Sons", second edition, 1988.

[14] N. Bohr: *On the theory of the decrease of velocity of moving electrified particles on passing through matter*. Philosophical Magazine Series 6, 25(145):10–31, 1913.

[15] J. F. Ziegler, J. P. Biersack, M. Ziegler, D. J. Marwick, G. A. Cuomo, W. A. Porter, and S. A. Harrison: *SRIM 2011 code*, 1984-2011. http://www.srim.org.

[16] A. Javanainen, T. Malkiewicz, J. Perkowski, W.H. Trzaska, A. Virtanen, G. Berger, W. Hajdas, R. Harboe-Sorensen, H. Kettunen, V. Lyapin, M. Mutterer, A. Pirojenko, I. Riihimaki, T. Sajavaara, G. Tyurin, and H.J. Whitlow: *Linear energy transfer of heavy ions in silicon*. Nuclear Science, IEEE Transactions on, 54(4):1158 –1162, 2007, ISSN 0018-9499.

[17] J. S. Lilley: *Nuclear physics: Principles and applications*, page 23.

[18] Geant4 Collaboration: *Validation and verification of electromagnetic physics*.

[19] M.A. Xapsos: *Applicability of LET to single events in microelectronic structures*. Nuclear Science, IEEE Transactions on, 39(6):1613–1621, dec 1992, ISSN 0018-9499.

[20] F. Yang and J.H. Hamilton: *Modern Atomic and Nuclear Physics*. WORLD SCIENTIFIC PUB CO (, 2009, ISBN 9789812836786. http://books.google.fi/books?id=LXv8Xh3GE6oC.

[21] G. Santin, D. Wright, and M Asai: *Space radiation transport models*. Nuclear and Space Radiation Effects Conference, Short Course Notebook, Section III, 2006.

[22] S. A. Bass *et al.*: *Microscopic models for ultrarelativistic heavy ion collisions*. Prog. Part. Nucl. Phys., 41:255–369, 1998.

[23] *Neutron-induced 10b fission as a major source of soft errors in high density srams*. Microelectronics Reliability, 41(2):211–218, 2001, ISSN 0026-2714.

[24] Wikipedia: *Nuclear binding energy*.

[25] E. B. Podgorsak: *Radiation Oncology Physics: A Handbook for Teachers And Students*. International Atomic Energy Agency, ISBN 9201073046.

[26] R.P. Haviland: *Emulating the solar cycle*. Antennas and Propagation Magazine, IEEE, 38(5):38 –44, October 1996, ISSN 1045-9243.

[27] S. Bourdarie: *From space environment to specifications*. RADECS Short Course, 2011.

[28] T. Salminen: *Avaruussäteilyn aiheuttamista virheistä elektroniikkakomponenteissa, MSc. Thesis*. 2004.

[29] J. L. Barth: *The evolution of the radiation environments*. RADECS Short Course, 2009.

[30] NASA Space Radiation Analysis Group, Johnson Space Center: *What is space radiation?*

[31] E.J. Daly, J. Lemaire, D. Heynderickx, and D.J. Rodgers: *Problems with models of the radiation belts*. Nuclear Science, IEEE Transactions on, 43(2):403 –415, apr 1996, ISSN 0018-9499.

[32] NASA: *South atlantic anomaly*. http://heasarc.gsfc.nasa.gov/docs/rosat/gallery/misc_saad.html, October 2011.

[33] T. K. Gaisser: *Cosmic Rays and Particle Physics*. Cambridge University Press, Cambridge, 1990.

[34] U. Bravar, E.O. Fluckiger, K. Godin, Z.C. Hansen, J.R. Macri, M.L. McConnell, R.S. Miller, M.R. Moser, and J.M. Ryan: *Atmospheric neutron measurements with the sontrac science model*. In *Nuclear Science Symposium Conference Record, 2005 IEEE*, volume 2, pages 634 –638, 2005.

[35] Wikipedia: *Cosmic ray*.

[36] John W. Wilson, F. A. Cucinotta, J. L. Shinn, L. C. Simonsen, R. R. Dubey, W. R. Jordan, T. D. Jones, C. K. Chang, and M. Y. Kim: *Shielding from solar particle event exposures in deep space*. Radiation Measurements, 30(3):361–382, 1999, ISSN 1350-4487.

[37] K. Avery: *Radiation effects point of view*. Nuclear and Space Radiation Effects Conference, Short Course Notebook, Section II, 2009.

[38] J. R. Srour, C. J. Marshall, and P. W. Marshall: *Review of displacement damage effects in silicon devices*. Nuclear Science, IEEE Transactions on, 50(3):653 – 670, 2003, ISSN 0018-9499.

[39] A. Paccagnella and S. Gerardin: *Basics of radiation effects in electronic devices*. RADECS Short Course, 2009.

[40] H. J. Barnaby: *Total-Dose Effects in Modern Integrated Circuit Technologies*. Nuclear and Space Radiation Effects Conference, Short Course Notebook, Section III, 2005.

[41] NASA/GSFC Radiation Effects & Analysis: *Single event effect specification*. http://radhome.gsfc.nasa.gov/radhome/papers/seespec.htm, December 2010.

[42] P. E. Dodd, F. W. Sexton, G. L. Hash, M. R. Shaneyfelt, B. L. Draper, A. J. Farino, and R. S. Flores: *Impact of technology trends on seu in cmos srams*. Nuclear Science, IEEE Transactions on, 43(6):2797 –2804, December 1996, ISSN 0018-9499.

[43] P. E. Dodd and L .W. Massengill: *Basic mechanisms and modeling of single-event upset in digital microelectronics*. Nuclear Science, IEEE Transactions on, 50(3):583 – 602, 2003, ISSN 0018-9499.

[44] Wikipedia: *Static random-access memory*.

[45] E. Petersen: *Soft error results analysis and error rate prediction*. Nuclear and Space Radiation Effects Conference, Short Course Notebook, Section III, 2008.

[46] R. Silberberg, C. H. Tsao, and J. R. Letaw: *Neutron generated single-event upsets in the atmosphere*. Nuclear Science, IEEE Transactions on, 31(6):1183 –1185, 1984, ISSN 0018-9499.

[47] A. H Taber and E. Normand: *Investigation and characterization of seu effects and hardening strategies in avionics*. Boeing Defense and Space Group Seattle Wa.

[48] L Talbot: *Cosmic radiation and aircrew exposure: Implementation of european requirements in civil aviation*. Journal of Radiological Protection, 19(1).

[49] M. Alles: *Process technology and hardening*. Nuclear and Space Radiation Effects Conference, Short Course Notebook, Section I, 2007.

[50] J. C. Pickel and J. T. Blandford: *Cosmic Ray Induced in MOS Memory Cells*. Nuclear Science, IEEE Transactions on, 25(6):1166 –1171, dec. 1978, ISSN 0018-9499.

[51] John N. Bradford: *Geometric Analysis of Soft Errors and Oxide Damage Produced by Heavy Cosmic Rays and Alpha Particles*. Nuclear Science, IEEE Transactions on, 27(1):941 –947, feb. 1980, ISSN 0018-9499.

[52] E.L. Petersen, V. Pouget, L.W. Massengill, S.P. Buchner, and D. McMorrow: *Rate predictions for single-event effects - critique ii*. Nuclear Science, IEEE Transactions on, 52(6):2158 – 2167, 2005, ISSN 0018-9499.

[53] R. Harboe-Sorensen, L. Adams, E. J. Daly, C. Sansoe, D. Mapper, and T. K. Sanderson: *The SEU Risk Assessment of Z80A, 8086 and 80C86 Microprocessors Intended for Use in a Low Altitude Polar Orbit*. Nuclear Science, IEEE Transactions on, 33(6):1626 –1631, dec. 1986, ISSN 0018-9499.

[54] E. L. Petersen, J. C. Pickel, Jr. Adams, J. H., and E. C. Smith: *Rate prediction for single event effects-a critique*. Nuclear Science, IEEE Transactions on, 39(6):1577 –1599, dec 1992, ISSN 0018-9499.

[55] D. Binder: *Analytic seu rate calculation compared to space data*. Nuclear Science, IEEE Transactions on, 35(6):1570 –1572, dec 1988, ISSN 0018-9499.

[56] V. V. Miroshkin and M. G. Tverskoy: *Two parameter model for predicting SEU rate [memory devices]*. Nuclear Science, IEEE Transactions on, 41(6):2085 –2092, dec 1994, ISSN 0018-9499.

[57] E.L. Petersen: *Predictions and observations of seu rates in space*. Nuclear Science, IEEE Transactions on, 44(6):2174 –2187, December 1997, ISSN 0018-9499.

[58] K.M. Warren, R.A. Weller, M.H. Mendenhall, R.A. Reed, D.R. Ball, C.L. Howe, B.D. Olson, M.L. Alles, L.W. Massengill, R.D. Schrimpf, N.F. Haddad, S.E. Doyle, D. McMorrow, J.S. Melinger, and W.T. Lotshaw: *The contribution of nuclear reactions to heavy ion single event upset cross-section measurements in a high-density seu hardened sram*. Nuclear Science, IEEE Transactions on, 52(6):2125 – 2131, 2005, ISSN 0018-9499.

[59] R. A. Reed, R. A. Weller, R. D. Schrimpf, M. H. Mendenhall, K. M. Warren, and L. W. Massengill: *Implications of nuclear reactions for single event effects test methods and analysis*. Nuclear Science, IEEE Transactions on, 53(6):3356 –3362, 2006, ISSN 0018-9499.

[60] P. E. Dodd, J. R. Schwank, M. R. Shaneyfelt, J. A. Felix, P. Paillet, V. Ferlet-Cavrois, J. Baggio, R. A. Reed, K. M. Warren, R. A. Weller, R. D. Schrimpf, G. L. Hash, S. M. Dalton, K. Hirose, and H. Saito: *Impact of Heavy Ion Energy and Nuclear Interactions on Single-Event Upset and Latchup in Integrated Circuits*. Nuclear Science, IEEE Transactions on, 54(6):2303 –2311, dec. 2007, ISSN 0018-9499.

[61] P.E. Dodd, M.R. Shaneyfelt, J.R. Schwank, and J.A. Felix: *Current and Future Challenges in Radiation Effects on CMOS Electronics*. Nuclear Science, IEEE Transactions on, 57(4):1747 –1763, 2010, ISSN 0018-9499.

[62] L. Borucki, G. Schindlbeck, and C. Slayman: *Comparison of accelerated DRAM soft error rates measured at component and system level*. In *Reliability Physics Symposium, 2008. IRPS 2008. IEEE International*, pages 482 –487, 27 2008-may 1 2008.

[63] D. F. Heidel, P. W. Marshall, K. A. LaBel, J. R. Schwank, K. P. Rodbell, M. C. Hakey, M. D. Berg, P. E. Dodd, M. R. Friendlich, A. D. Phan, C. M. Seidleck, M. R. Shaneyfelt, and M. A. Xapsos: *Low energy proton single-event-upset test results on 65 nm soi sram*. Nuclear Science, IEEE Transactions on, 55(6):3394 –3400, 2008, ISSN 0018-9499.

[64] D.F. Heidel, P.W. Marshall, J.A. Pellish, K.P. Rodbell, K.A. LaBel, J.R. Schwank, S.E. Rauch, M.C. Hakey, M.D. Berg, C.M. Castaneda, P.E. Dodd, M.R. Friendlich, A.D. Phan, C.M. Seidleck, M.R. Shaneyfelt, and M.A. Xapsos: *Single-event upsets and multiple-bit upsets on a 45 nm soi sram*. Nuclear Science, IEEE Transactions on, 56(6):3499 –3504, 2009, ISSN 0018-9499.

[65] B. D. Sierawski, M. H. Mendenhall, R. A. Reed, M. A. Clemens, R. A. Weller, R. D. Schrimpf, E. W. Blackmore, M. Trinczek, B. Hitti, J. A. Pellish, R. C. Baumann, Shi Jie Wen, R. Wong, and N. Tam: *Muon-Induced Single Event Upsets in Deep-Submicron Technology, year=2010*. Nuclear Science, IEEE Transactions on, 57(6):3273 –3278, ISSN 0018-9499.

[66] R. A. Reed, J. Kinnison, J. C. Pickel, S. Buchner, P. W. Marshall, S. Kniffin, and K. A. LaBel: *Single-event effects ground testing and on-orbit rate prediction methods: the past, present, and future*. Nuclear Science, IEEE Transactions on, 50(3):622 – 634, 2003, ISSN 0018-9499.

[67] M. P. King, R. A. Reed, R. A. Weller, M. H. Mendenhall, R. D. Schrimpf, M. L. Alles, E. C. Auden, S. E. Armstrong, and M. Asai: *The Impact of Delta-Rays on Single-Event Upsets in Highly Scaled SOI SRAMs*. Nuclear Science, IEEE Transactions on, 57(6):3169 –3175, 2010, ISSN 0018-9499.

[68] P. E. Dodd, O. Musseau, M. R. Shaneyfelt, F. W. Sexton, C. D'hose, G. L. Hash, M. Martinez, R. A. Loemker, J. L. Leray, and P. S. Winokur: *Impact of ion energy on single-event upset*. Nuclear Science, IEEE Transactions on, 45(6):2483 –2491, December 1998, ISSN 0018-9499.

[69] M. A. Clemens, N. C. Hooten, V. Ramachandran, N. A. Dodds, R. A. Weller, M. H. Mendenhall, R. A. Reed, P. E. Dodd, M. R. Shaneyfelt, J. R. Schwank, and E. W. Blackmore: *The Effect of High-Z Materials on Proton-Induced Charge Collection*. Nuclear Science, IEEE Transactions on, 57(6):3212 –3218, dec. 2010, ISSN 0018-9499.

[70] R.A. Weller, M.H. Mendenhall, R.A. Reed, R.D. Schrimpf, K.M. Warren, B.D. Sierawski, and L.W. Massengill: *Monte carlo simulation of single event effects*. Nuclear Science, IEEE Transactions on, 57(4):1726 –1746, 2010, ISSN 0018-9499.

[71] R. A. Weller and R. A. Reed: *Single Event Effects in Microelectronics*. A presentation in the Summer School at the Department of Physics, University of Jyväskylä, 2010.

[72] R.A. Reed, R.A. Weller, M.H. Mendenhall, J. M. Lauenstein, K.M. Warren, J.A. Pellish, R.D. Schrimpf, B.D. Sierawski, L.W. Massengill, P.E. Dodd, M.R. Shaneyfelt, J.A. Felix, J.R. Schwank, N.F. Haddad, R.K. Lawrence, J.H. Bowman, and R. Conde: *Impact of ion energy and species on single event effects analysis*. Nuclear Science, IEEE Transactions on, 54(6):2312 –2321, dec. 2007, ISSN 0018-9499.

[73] K. M. Warren, A. L. Sternberg, R. A. Weller, M. P. Baze, L. W. Massengill, R. A. Reed, M. H. Mendenhall, and R. D. Schrimpf: *Integrating Circuit Level Simulation and Monte-Carlo Radiation Transport Code for Single Event Upset Analysis in SEU Hardened Circuitry*. Nuclear Science, IEEE Transactions on, 55(6):2886 –2894, 2008, ISSN 0018-9499.

[74] D. R. Ball, K. M. Warren, R. A. Weller, R. A. Reed, A. Kobayashi, J. A. Pellish, M. H. Mendenhall, C. L. Howe, L. W. Massengill, R. D. Schrimpf, and N. F. Haddad: *Simulating nuclear events in a tcad model of a high-density seu hardened sram technology*. Nuclear Science, IEEE Transactions on, 53(4):1794 –1798, 2006, ISSN 0018-9499.

[75] *G4–a simulation toolkit*. Nuclear Instruments and Methods in Physics Research Section A: Accelerators, Spectrometers, Detectors and Associated Equipment, 506(3):250 – 303, 2003, ISSN 0168-9002.

[76] *Geant4 web page*. http://geant4.cern.ch/.

[77] QinetiQ: *MUlti-LAyered Shielding SImulation Software*. http://reat.space.qinetiq.com/mulassis/, December 2010.

[78] F. Lei, R. R. Truscott, C. S. Dyer, B. Quaghebeur, D. Heynderickx, R. Nieminen, H. Evans, and E. Daly: *MULASSIS: a Geant4-based multilayered shielding simulation tool*. Nuclear Science, IEEE Transactions on, 49(6):2788 – 2793, December 2002, ISSN 0018-9499.

[79] European Space Agency and Belgian Institute for Space Aeronomy: *Space Environment, Effects, and Education System*. http://www.spenvis.oma.be/, December 2010.

[80] D. Heynderickx, B. Quaghebeur, J. Wera, E. J. Daly, and H. D. R. Evans: *New radiation environment and effects models in ESA's space environment information system (SPENVIS)*. In *Radiation and Its Effects on Components and Systems, 2003. RADECS 2003. Proceedings of the 7th European Conference on*, pages 643 – 646, 2003.

[81] T. J. Roberts and D. M. Kaplan: *G4beamline simulation program for matter-dominated beamlines*. In *Particle Accelerator Conference, 2007. PAC. IEEE*, pages 3468 –3470, 2007.

[82] Geant4 Collaboration: *Geant4 User's Guide for Application Developers*.

[83] V. Ivantchenko: *Recent Improvements in Geant4 Electromagnetic Physics Models and Interfaces*. proceedings of the Joint International Conference on Supercomputing in Nuclear Applications and Monte Carlo 2010.

[84] Geant4 Collaboration: *Geant4 Physics Reference Manual*.

[85] R. A. Weller, M. H. Mendenhall, and D. M. Fleetwood: *A screened Coulomb scattering module for displacement damage computations in Geant4*. Nuclear Science, IEEE Transactions on, 51(6):3669 – 3678, 2004, ISSN 0018-9499.

[86] K. Amako, S. Guatelli, V. N. Ivanchenko, M. Maire, B. Mascialino, K. Murakami, P. Nieminen, L. Pandola, S. Parlati, M. G. Pia, M. Piergentili, T. Sasaki, and L. Urban: *Comparison of Geant4 Electromagnetic Physics Models Against the NIST Reference Data*. Nuclear Science, IEEE Transactions on, 52(4):910 – 918, 2005, ISSN 0018-9499.

[87] T Toshito *et al.*: *New Geant4 Electromagnetic Physics Developments for Ion Therapy Applications*. proceedings of the Joint International Conference on Supercomputing in Nuclear Applications and Monte Carlo 2010.

[88] P. Degtyarenko, M. Kossov, and H. Wellisch: *Chiral invariant phase space event generator*. The European Physical Journal A - Hadrons and Nuclei, 8:217–222, ISSN 1434-6001.

[89] V. Uzhinsky: *Development of the Fritiof Model in Geant4*. proceedings of the Joint International Conference on Supercomputing in Nuclear Applications and Monte Carlo 2010.

[90] K. Niita, T. Maruyama, Y. Nara, S. Chiba, and A. Iwamoto: *Development of JQMD (Jaeri Quantum Molecular Dynamics) Code*. Nippon Genshiryoku Kenkyujo JAERI,Data,Code, 1999.

[91] T. Koi, M. Asai, D.H. Wright, K. Niita, Y. Nara, K. Amako, and T. Sasaki: *Interfacing the JQMD and JAM Nuclear Reaction Codes to Geant4*. Conference for Computing in High-Energy and Nuclear Physics (CHEP 03, 2003.

[92] Koji Niita, Satoshi Chiba, Toshiki Maruyama, Tomoyuki Maruyama, Hiroshi Takada, Tokio Fukahori, Yasuaki Nakahara, and Akira Iwamoto: *Analysis of the (N,xN') reactions by quantum molecular dynamics plus statistical decay model*. Phys. Rev. C, 52(5):2620–2635, Nov 1995.

[93] T. Koi: *New native QMD code in Geant4*. proceedings of the Joint International Conference on Supercomputing in Nuclear Applications and Monte Carlo 2010.

[94] G. Folger, V. N. Ivanchenko, and J. P. Wellisch: *The Binary Cascade*. The European Physical Journal A - Hadrons and Nuclei, 21:407–417, ISSN 1434-6001.

[95] D. H. Wright, T. Koi, G. Folger, V. Ivanchenko, M. Kossov, N. Starkov, A. Heikkinen, and Wellisch H.: *Low and High Energy Modeling in Geant4*.

[96] D. H. Wright: *An Overview of Geant4 Hadronic Physics Improvements*. proceedings of the Joint International Conference on Supercomputing in Nuclear Applications and Monte Carlo 2010.

[97] R. A. Weller, R. A. Reed, Schrimpf R. D., and Massengill L. W: *Fundamental aspects of radiation event generation for electronics and engineering research*.

[98] T Koi: *Hadron Physics II*. in Geant4 Tutorial at Texas A& M, 2011.

[99] M. H. Mendenhall: *Heavy nucleus fragmentation theory and experiment and its importance to understanding the space environment*. In Geant4 Space Users and Spenvis Users Workshop, 2006.

[100] K. Kwiatkowski, S. H. Zhou, T. E. Ward, V. E. Viola, H. Breuer, G. J. Mathews, A. Gökmen, and A. C. Mignerey: *Energy Deposition in Intermediate-Energy Nucleon-Nucleus Collisions*. Phys. Rev. Lett., 50(21):1648–1651, May 1983.

[101] J. Wehner: *Monte Carlo simulation of an ion production ring for a beta beam neutrino facility*, 2009.

[102] A. Lechner, V.N. Ivanchenko, and J. Knobloch: *Validation of recent Geant4 physics models for application in carbon ion therapy*. Nuclear Instruments and Methods in Physics Research Section B: Beam Interactions with Materials and Atoms, 268(14):2343–2354, 2010, ISSN 0168-583X.